Department of Environmental Science and Engineering

College of Engineering

Tunghai University

Master Thesis

以水熱法合成之硫化銅作為可見光觸媒降解水中巴拉刈

Hydrothermal Synthesis of CuS as Photocatalyst to Degrade Paraquat via Heterogeneous Photo-Fenton-like Oxidation under Visible Light

Hui-Chun Lee

Advisor: Walter Den, Ph.D., Tunghai University

Co- advisor：Nurak Grisdanurak, Ph.D., Thammasat University

November, 2016

東海大學碩士班研究生

論文指導教授推薦書

環境科學與工程學系李蕙君君所提之論文

題目：以水熱法合成之硫化銅作為可見光觸媒降解水中巴拉刈

Hydrothermal Synthesis of CuS as Photocatalyst to Degrade Paraquat via Heterogeneous Photo-Fenton-like Oxidation under Visible Light

係由本人指導撰述，同意提付審查。

指導教授：鄭宇辰（簽章）

105年9月20日

東海大學環境科學系碩士班

論文口試委員審定書

環境科學與工程學系碩士班李蕙君君所提之論文

題目：以水熱法合成之硫化銅作為可見光觸媒降解水中巴拉刈

Hydrothermal Synthesis of CuS as Photocatalyst to Degrade Paraquat via Heterogeneous Photo-Fenton-like Oxidation under Visible Light

---

經本委員會審議，認為符合碩士資格標準。

論文口試委員召集人 陳志成 （簽章）

委員 鄭宗憲

林坤儀

陳志成

中華民國 105 年 9 月 6 日

誌謝

將近五年的研究生涯完成了兩個里程碑，從在東海剛升為大三生時就已經在指導教授 鄧宗禹老師的空污奈米實驗室學習專題研究，大學專題「螺旋藻去除水中酚」也投稿成國外期刊論文。大學畢業後讀碩士繼續當鄧老師的研究生，碩士這兩年研究題目，經四處摸索(微藻、污泥、奈米碳管)後，而投入關於 3D 石墨烯/奈米碳管之研究，但後來因緣際會下泰國 Nurak 老師邀請學生至泰國法政大學(Thammasat University)化學工程系進行研究交流三個月，方此而定了最後的研究方向。

首先要感謝鄧老師這四年多亦師亦友的指導、教誨與鼓勵並總是很放心地讓學生自由發揮做研究，也因而讓學生對研究可以是真的有興趣而喜歡做研究，亦感謝系上所有老師的同意以及 Nurak 老師的邀請且在泰國的指導與照顧，讓學生能至國外研究交流拓展視野，學習讓自己變更好也更確定自己的未來。還有感謝在出國前陳維燁老師說的話，問說：「妳是要去泰國玩?」，學生說「當然不是去玩而是做研究，然後有空閒的話才去玩。」老師則說：「做研究也是玩啊！」，頓時當頭棒喝，從大三開始即喜歡做研究，沒錯！就是在玩，遇到問題找文獻資料來解決問題時很開心！做實驗不論成或敗都是結果都有成就感！所以只要心態正向愉快並充實了自己，做什麼事情都是在玩，玩研究、玩生活！感謝在本論文口試期間，承蒙逢甲大學　陳志成老師、中興大學　林坤儀老師於口試時，提出許多寶貴的建議，讓學生的研究能夠更完整。

感謝泰國法政大學 Nurak 老師 Cat. Lab 的 Pi Fa、Pi Kwan、Pi Eddy、Pi Ah、Yui、Tum、Aumz、Nantan、Dek 的照顧，特別是 Pi Kwan 像姐姐般的照料與被說長相像姊妹的 Yui 實驗好夥伴在實驗與生活上一路陪伴。更感謝第二個家—空污奈米實驗室的夥伴們，小孟學姐、采薇學姊、薇馥學姊、雅琪學姊、駱博、企鵝學長、宗哲學長、陳大哥、蘇大哥、Pi New、Pi Ekk、欣慈、柏穎、栢諺、柏勳、瑞珂、大蝦、妶妏、虹雯、昱蓉，四年多的生活有你們參與很榮幸，有哭有笑都經歷過，因為有你們的相處所以珍愛實驗室，謝謝大家的體諒與體貼，尤其是在泰國期間，辛苦栢諺與柏勳一起支撐著實驗室讓我可以專心完成實驗與論文，沒有大家的幫忙就沒有這份完整的論文。也謝謝系辦阿梅學姊、美君學姊、欣怡學姐在課堂與其他事物上的協助，謝謝其他實驗室朋友阿均、阿杜、琮琮、太陽、卓卓、阿蘇、翁笛的隨揪隨到好溫馨，謝謝朋友阿雞、阿姿、肥如、雅偵、小于的陪伴與支持。

最後，最感謝家人，在求學生涯中，因為父親汗流浹背日曬雨淋不斷地付出與叮嚀、母親與姊姊哥哥也在背後不斷的支持、勉勵及體諒犧牲與你們相處的時間，使我可以專注地在學業上並順利完成學業，也最感謝這個孕育美麗環境的地球與造物者 上帝，才能成就得了現在的李蕙君，所有的感激無法言喻，今僅將此論文獻給我所感激的人。

李蕙君　謹誌

2016 年 11 月　東海大學

ABSTRACT (CHINESE)

本研究目的欲利用水熱法合成硫化銅(CuS)，並作為可見光觸媒結合類芬頓法(Fenton-like)降解水中除草劑「巴拉刈」。實驗以氯化銅($CuCl_2 \cdot 2H_2O$)、硫化鈉($Na_2S \cdot 9H_2O$)與界面活性劑溴化十六烷基三甲銨(Cetyltrimethyl ammonium bromide，CTAB)在不同反應時間(24、48 及 72 小時)、不同銅硫莫耳比(1：6、1：8 及 1：10)及固定溫度(130℃)條件下合成九種硫化銅顆粒。合成之 CuS 以 X 光繞射、掃描電子顯微鏡以及紫外-可見漫反射光譜來分析物理特性。CuS 的晶體結構是六方晶相且晶體尺寸為 25.89-38.40 nm，能帶隙(Energy band-gap)在 1.88-2.04 eV。顆粒大小範圍為 250-500 nm，其型態變化隨著硫含量與反應時間增加而複雜，從顆粒狀變平板狀與多層結構。

於可見光照射下並添加過氧化氫(H_2O_2)降解水中巴拉刈探討 CuS 的光催化活性，結果顯示九種 CuS 在 240 分鐘內皆能去除 100% 初始濃度為 40 mg/L 的巴拉刈且降解效能比商業二氧化鈦(TiO_2 P25)為佳。其中以銅硫莫耳比 1:8 合成 72 小時的 CuS 擁有最佳降解效益，以擬一階反應方程式推演其直接光解反應速率常數(k_{obs})為 2.0×10^{-2} /min 及初始反應速率(r_0)為 0.251×10^{-2} mM/min。CuS 光降解巴拉刈屬於異相光催化符合 Langmuir-Hinshelwood 動力模式之型態，推導而得反應物的吸附速率常數(K_a)為 10.34 /mM 、光催化表面反應速率常數(k_r) 為 2.5×10^{-3} /min。在可見光觸媒結合類芬頓法的降解系統中，添加過氧化氫(H_2O_2)可以克服 CuS 顆粒內部電荷重組問題並生成更多的氫氧自由基($^{\bullet}OH$)而促進光催化活性。本系統中藉由兩種方式降解巴拉刈，一是由 CuS 顆粒表面電子-電洞的氧化還原反應直接分解；另一種則透過液相中氫氧自由基($^{\bullet}OH$)氧化的間接分解。

關鍵字：硫化銅、巴拉刈、過氧化氫、光降解機制、動力學

ABSTRACT (ENGLISH)

Copper(II) sulfide photocatalysts were successfully synthesized by hydrothermal method from the solution of $CuCl_2 \cdot 2H_2O$ and $Na_2S \cdot 9H_2O$ at 130℃, with cetyltrimethyl ammonium bromide (CTAB) as a reducing agent, and the synthetic parameters such as reaction time (24 h, 48 h and 72 h) and molar ratio of copper-to-sulfur (1:6, 1:8 and 1:10).

The products were characterized by X-ray diffraction (XRD), scanning electron microscopy (SEM) and UV-Vis diffuse reflectance (UV-DR) spectroscopy. The XRD peaks were indexed to the pattern of hexagonal phase of CuS and crystallite size were 25.89-38.40 nm. The particles size ranged from 250 to 500 nm. Energy band-gap was in range of 1.88–2.04 eV. The more complex structures (plate, rope-like and hierarchical structure) were obtained with increased sulfur content and reaction times.

The photocatalytic activity was evaluated observing degradation of paraquat solution under visible light. The results showed that 100 % removal within 240 min was obtained for solution containing an initial concentration of 40 mg/L paraquat. CuS has better photocatalytic performance then the commercial TiO_2 P25 in the presence of H_2O_2.

CuS achieved an optimal photocatalytic performance when Cu:S equal 1:8 via hydrothermal treatment for 72 h, and followed a pseudo-first order with an observed rate constant (k_{obs}) of 2.0×10^{-2} /min and an initial reaction rate (r_0) of 0.251×10^{-2} mM/min. The photocatalytic degradation of paraquat kinetic model fit well with the Langmuir-Hinshelwood adsorption equilibrium constant (K_a) of

10.34 /mM and the surface reaction rate constant (k_r) of 2.5×10^{-3} /min expressed by Langmuir–Hinshelwood rate law.

The presence of H_2O_2 in heterogeneous photo-Fenton-like system improved the photocatalytic activity due to overcomes the charge recombination in CuS when H_2O_2 as an electron acceptor and generates more hydroxyl radicals. It has two ways to decompose paraquat. One is direct decomposition via redox reactions from electron-hole pairs on the CuS surface. Another one is indirect decomposition by hydroxyl radicals ($OH^{\bullet}$) in surroundings solution.

Keywords: Copper sulfide, Paraquat, Hydrogen peroxide, Photocatalytic degradation mechanism, Kinetic

TABLE OF CONTENT

LIST OF FIGURES

LIST OF TABLES

Chapter 1 Introduction

1.1 Background

Copper sulfide has attracted interest because it has optical, electronic, physical and chemical properties (Wang et al., 2014b). It can be applied to use in many applications such as p-type semiconductor in solar cell (Gordon et al., 2015), adsorption and commonly applied as catalyst. Copper sulfide has many formulas such as covellite (CuS), chalcocite (Cu_2S) and villamaninite (CuS_2). Therefore, it can be prepared for many methods such as solvothermal (Shamraiz et al., 2016), microwave irradiation (Yan et al., 2013), sonication (Mousavi-Kamazani et al., 2013), sol-gel precipitation (Gurin et al., 2003) and hydrothermal (Saranya et al., 2014b). In comparison with other methods to synthesize copper sulfide, hydrothermal is a simpler, low cost and friendly to environment.

Copper sulfide has a direct energy band-gap of around 1.27 - 1.75 eV (Pop et al., 2011). The narrow band-gap can efficiently utilize the visible region ($\lambda >$ 400 nm) which covers the largest proportion of the solar spectrum. It is visible-light-driven (VLD) photocatalysts that can be widely applied in photocatalytic degradation of organic compounds. Saranya *et al*. (2014a) reported that the photocatalytic activity was evaluated by the decolorization of methylene blue (20 mg/L) under visible-light irradiation and showed that 87% of the dye was degraded after 40 min. CuS is one of the excellent photocatalysts for degradation of dye, the order of decolorization under solar light efficiency of

various photocatalysts is CuS > ZnO > FeO > CdS > NiS > ZnS > CdO > NiO > FeS (Nezamzadeh-Ejhieh and Moazzeni, 2013).

Photocatalysis and Fenton-like oxidation is one of advanced oxidation process (AOPs). AOPs is an efficient way to solve pollution problems for different reacting systems based on the generation of extremely reactive and non-selective oxidizing hydroxyl radicals (Glaze et al., 1987). The presence of electron acceptor such as hydrogen peroxide or oxygen can overcome the drawbacks of electron-hole recombination which is easy occurred in narrow band-gap semiconductors (Nimtz, 1980), further promote photogeneration of hydroxyl radicals (Miguel et al., 2012).

Therefore, our study selected CuS as photocatalyst and introduced into heterogeneous photo-Fenton-like oxidation system. In this study, factors influencing synthesis and photocatalysis of copper sulfide nanoparticles were investigated. Firstly, copper sulfide nanoparticles were fabricated by hydrothermal method. Characterizations of copper sulfide by X-ray diffraction (XRD), scanning electron microscopy (SEM) and UV-Vis diffuse reflectance (UV-DR) spectroscopy were applied to confirm the formulas and properties. In addition, photodegradable experiments on paraquat solution as a pollutant probe were presented. Finally, temperature, time and ratio affecting copper sulfide synthesis were observed through its characteristics and photocatalytic activity.

1.2 Objectives

- To synthesize CuS nanocrystals utilizing hydrothermal method and study characteristic of CuS including to investigate the sulfur content and synthesis time affecting the morphology.
- To study the semiconductor "CuS" as photocatalyst to degrade the herbicide "paraqaut" via heterogeneous photo-Fenton-like oxidation under visible light.

1.3 Scopes of Study

- The preparation of CuS nanocrystals by hydrothermal method was modified from Zhang's method (2008). The composition of synthesized catalysts includes :

  - Molar ratios of copper (Cu) to sulfur (S): 1:6, 1:8, 1:10
  - Synthesis time (h): 24, 48, 72
  - Synthesis temperature (°C): 130

- Photocatalytic activity evaluation:

  - Concentration of paraquat solution: 20, 40, 60, 80, 100 mg/L
  - Volume of paraquat solution: 40 mL
  - Catalysts dosage: 1.0 g/L
  - Hydrogen peroxide (H_2O_2) dosage: 0.22 M
  - Time: dark for 60 min then visible light irradiation for 240 min
  - Visible light irradiance: 6 W/m^2

Chapter 2 Literature Review

One of the increasingly severe challenges in chemistry is diminishing the detrimental environmental impact associated with chemical industries. Advanced oxidation process (AOPs) is an efficient way to solve pollution problems for different reacting systems based on the generation of extremely reactive and non-selective oxidizing hydroxyl radicals ($^{\bullet}OH$) via Fenton, photo-Fenton reactions and photocatalysis. These have powerful capability to oxidize numerous organic compounds into small pollution-free compounds, CO_2 and H_2O. The versatility of AOP makes it very flexible to offer $^{\bullet}OH$ radicals for the specific treatment requirements (Glaze et al., 1987). Hydroxyl radicals are produced with the help of one or more primary oxidants (e.g. ozone, hydrogen peroxide and oxygen), energy sources (e.g. radiations) or catalysts (e.g. titanium dioxide, ferrous iron). Sunlight, a pollution-free and easily available energy resource, possesses great potential in driving environmentally benign organic transformations.

In this work, we have reviewed heterogeneous catalytic oxidation under radiation which is one of the AOPs. We considered about semiconductor as catalysts applied on photocatalysis combined with photo-Fenton-like reaction to degrade the organic contaminants in water.

2.1 Heterogeneous Catalytic Oxidation under Radiation

Heterogeneous catalytic oxidation has the catalyst in a different phase from the reactants. Especially for the AOP, the introduction of light is necessary for the photocatalysis and enhances dramatically the activity of Fenton reactions.

2.1.1 Semiconductor Photocatalysis

The catalyst was stimulated by using photon in order to decrease activation energy of the reaction. Photocatalysis is the acceleration of photoreaction in the presence of a catalyst. The photocatalysis commonly use semiconductor as a catalyst because it has band-gap energy (E_g) and can be used in photo degradation to degrade organic pollutant. Three components must be present in order for the photocatalytic reaction to take place: an emitted photon, a catalyst surface and a strong oxidizing agent. Suri et al. (1993) explained the mechanisms of heterogeneous photocatalytic reaction: When the semiconductor is irradiated under light, electrons (e^-) are excited from the valence band (VB) to the conduction band (CB) of the particles as the absorption of photon energy (hν) is higher than or equal to band-gap energy of the semiconductor, and leaves an electronic vacancy called a hole (h^+) in the VB (Eq. 2-1).

$$\text{Semiconductor} + h\nu \rightarrow e^- + h^+ \qquad \text{(Eq. 2-1)}$$

The photogenerated e^- and h^+ can either recombine in the solid, or transfer to the surface of semiconductor particle. At the surface, e^- and h^+ can take part in redox

reactions with adsorbed species (also called electron acceptors (A) and electron donors (D) in Fig. 2-1) such as water, OH^-, organic compounds and oxygen. The e^- takes part in reduction reactions with adsorbed oxygen to produce superoxide radicals ($^{\bullet}O_2^-$), which can produce hydrogen peroxide (H_2O_2) (Eq. 2-2) and hydroxyl radicals ($^{\bullet}OH$) (Eq. 2-3 to Eq. 2-6).

$$e^- + O_2 \rightarrow {}^{\bullet}O_2^- \quad \text{(Eq. 2-2)}$$

$$^{\bullet}O_2^- + H^+ \rightarrow HO_2^{\bullet} \quad \text{(Eq. 2-3)}$$

$$2HO_2^{\bullet} \rightarrow O_2 + H_2O_2 \quad \text{(Eq. 2-4)}$$

$$H_2O_2 + {}^{\bullet}O_2^- \rightarrow {}^{\bullet}OH + OH^- + O_2 \quad \text{(Eq. 2-5)}$$

$$H_2O_2 + h\nu \rightarrow 2HO^{\bullet} \quad \text{(Eq. 2-6)}$$

The $^{\bullet}OH$ are also formed by the reduction reactions of h^+ with water or OH^- (Eq. 2-7 and Eq. 2-8).

$$h^+ + H_2O \rightarrow {}^{\bullet}OH + H^+ \quad \text{(Eq. 2-7)}$$

$$h^+ + OH^- \rightarrow {}^{\bullet}OH \quad \text{(Eq. 2-8)}$$

The mechanism of semiconductor phtocatalysis is shown in Fig. 2-1: (I) the formation of charge carriers by a photon; (II) the charge carrier recombination to liberate heat; (III) the initiation of a reductive pathway by a conduction band electron; (IV) the initiation of an oxidative pathway by a valence band hole; (V) the further thermal (e.g., hydrolysis or reaction with active oxygen species) and photocatalytic reactions to yield mineralization products; (VI) the trapping of a

conduction band electron in a dangling surficial bond; (VII) the trapping of a valence-band hole at the surface of the semiconductor.

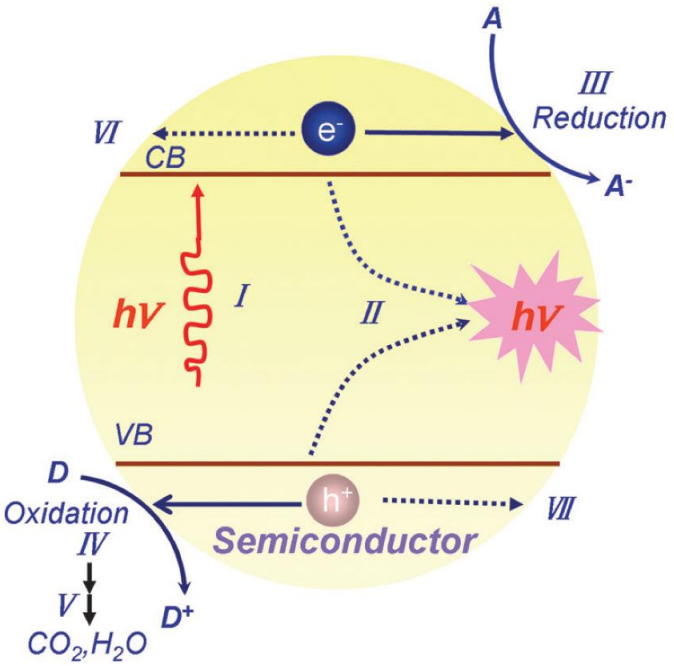

Fig. 2-1 Schematic illustration of semiconductor phtocatalysis (Wang et al., 2014a):

Overall, there has two ways to decompose organic compounds. One is direct decomposition via redox reactions from electron-hole pairs on the semiconductor surface. Another one is indirect decomposition by hydroxyl radicals ($^{\bullet}OH$) in surroundings (liquid or gas phase). In addition, it can add electron acceptors to overcome the drawback of fast charge recombination.

As the most famous photocatalyst, TiO_2 has been widely studied since Fujishima and Honda (1972) first reported the photoelectrochemical water-splitting on the TiO_2 electrode. However, the large energy gap (3.2 eV) makes TiO_2 can solely absorb the ultraviolet (UV) light, thus greatly depress the generation of hydroxyl radical which plays a key role in the oxidative destruction

of organic pollutant. But UV light occupies only 4% of the incoming solar light spectrum on the earth (Chen et al., 2010). To efficiently utilize the visible region (λ > 400 nm) which covers the largest proportion of the solar spectrum, the development of visible-light-driven (VLD) photocatalysts is the current trend. To achieve this goal, numerous semiconductors with narrow band-gap have been developed to solve the problem, such as Ag_2S (E_g=0.92 eV), Bi_2S_3 (E_g=1.3 eV), CuO (E_g=1.7 eV), CuS (E_g=1.9 eV), $BiFeO_3$ (E_g=2.05 eV), Fe_2O_3 (E_g=2.2 eV), WO_3 (E_g=2.7 eV), Bi_2WO_6 (E_g=2.8 eV) etc. (Xu and Schoonen, 2000). But the electron-hole recombination is easy occurred in narrow-gap semiconductors (Nimtz, 1980). Therefore, to overcome the serious drawbacks of fast charge recombination and the limited visible-light absorption of semiconductor photocatalysts, many strategies have been developed in the past few decades and the more widely used are to develop photocatalytic heterojunctions or combine with photo-Fenton reactions.

2.1.2 Heterogeneous Photo-Fenton-like Oxidation

In Fenton's reagent treatment (Fenton, 1894), owing to the necessary high dosage of iron and hydrogen peroxide, to achieve a high mineralization yield of the pollutant, as well as the continuous loss of catalyst and the important amount of generated iron hydroxide sludge, needing further separation. One of the most practical and interesting ways proposed to circumvent these limitations is the use of Fenton-like heterogeneous catalytic wet peroxide oxidation (Wang et al., 2016) with semiconductor photocatalysts and hydrogen peroxide (H_2O_2). Addition of

H_2O_2 as an electron acceptor on surface of semiconductor photocatalysts can enhance the photodegradation rate of organic pollutants due to overcomes the drawback of charge recombination (Kitsiou et al., 2009). An et al. (2013) investigated degradation of methyl violet (MV, 30 μmol/L), rhodamine B (RhB, 10 μmol/L) and phenol (3 mmol/L) in the $BiFeO_3$-H_2O_2-visible light (Vis) system with dosages ($BiFeO_3$ 0.5 g/L, H_2O_2 20, 10 and 60 mmol/L for the degradation of MV, RhB, and phenol, respectively). By introducing visible light irradiation, the degradation was significantly accelerated. For example, the MV removal within 120 min was increased from 49.8% in the dark to 91.3% under visible light irradiation. Mechakra et al. (2016) degraded 4.0×10^{-5} mol/L Linuron (3-[3,4-(dichlorophenyl)-1-methoxy-1-methylurea]) completely after 45 min using natural iron oxide (NIO) as a heterogeneous catalyst which consists mainly of iron oxide (α-Fe_2O_3) in the presence of H_2O_2 under fluorescent lamp.

Moreover, CuS is one of the excellent photocatalysts for degradation of dye, the order of decolorization efficiency of various photocatalysts is CuS > ZnO > FeO > CdS > NiS > ZnS > CdO > NiO > FeS (Nezamzadeh-Ejhieh and Moazzeni, 2013). Therefore, our study selected CuS as photocatalyst was introduced heterogeneous photo-Fenton-like oxidation system.

2.2 Copper Sulfide (Cu_xS_y)

Copper sulfide is an inorganic compound and black powder that is insoluble in water. The chemical compounds of copper sulfide are in the Cu_xS_y. copper sulfide can be prepared by many methods such as hydrothermal, solvothermal, aerosol, solution and thermolysis (Shamraiz et al., 2016). These methods can synthesize copper sulfide with different Cu and S ratio, time and temperature. Most formulas of the copper sulfide are covellite (CuS), chalcocite (Cu_2S) and villamaninite (CuS_2). Copper sulfide with specific morphology and size can be produced by different copper and sulfur source with the aid of assisting agent (Darouie et al., 2013). It has attracted interest because it has excellent physical and chemical properties. It can be applied to use in many applications such as p-type semiconductor in solar cell, adsorption and commonly applied as catalyst. All formulas of Cu_xS_y have been identified as p-type semiconductor materials. Copper sulfide has attracted attention because it has physical and chemical properties. Many research proposed many methods to synthesized copper sulfide, studied its optical properties and applied to use it in many applications. In Cu_xS_y, the most widely used in photodegradation of organic compounds is copper monosulfide (CuS).

2.2.1 **Synthesis of Copper(II) sulfide (CuS)**

Studies of CuS synthesis in last two decades are summarized in Table 2-1and Table 2-2. The direct energy band-gap ranges from 1.27 to 3.38 eV. The morphology of CuS has many forms like particle, plate, tube, hierarchical sphere. The widely used synthesis method are hydrothermal and solvothermal. In these two methods, CuS with specific morphology and size can be produced by different copper and sulfur source, surfactant, synthesis time and temperature.

For copper source, sulfur source and surfactant:

Kundu and Pradhan (2014) reported that CuS synthesis at 70℃ for 4 h with a 1:1 molar ratio of $Cu(NO_3)_2$ and $Na_2S_2O_3$, only CuS nanotubes was obtained; With a 2:1 molar ratio of $Cu(NO_3)_2$ and $Na_2S_2O_3$, both CuS nanotubes and nanoparticles were obtained; With a 1:2 $Cu(NO_3)_2$ and $Na_2S_2O_3$ molar ratio, there were no CuS nanotubes or other nanostructures. The diameter of CuS nanotubes formed in the presence of $CuSO_4$ (~ 400 nm) is found to be larger than that obtained with $Cu(NO_3)_2$ (< 200 nm). With $CuCl_2$ and $Na_2S_2O_3$, no nanotubes were obtained. The structures obtained with $CuCl_2$ and $Na_2S_2O_3$ precursors are the agglomeration of nanoflakes with a thickness < 25 nm. With $Cu(OAc)_2$ and $Na_2S_2O_3$, CuS nanoparticles are formed instead of nanotubes or nanoflakes

Thuy et al. (2014) synthesized CuS at 60℃ for 10 min with different Cu:S (Cu: $Cu(NO_3)_2 \cdot 3H_2O$, S: CH_3CSNH_2) molar ratio from 1:1, 1:2 to 1:4 gradually transforms particles from a nanoplate shape with broad size distribution to more well defined nanoplates and then to spherical nanoparticles of size 20–50 nm. In addition the particle size distribution narrows as the S content is increased, due to

CH_3CSNH_2 influencing both CuS nanocrystal nucleation and growth process, by initiating CuS nanocrystals formation and also acting as a surfactant to influence the reaction kinetics. Hence at high Cu:S ratios (Cu-rich) CH_3CSNH_2 acts only as the sulfur precursor forming CuS particle with non-uniform size. The fact crystallite size from XRD is invariant of Cu:S ratio suggests these particles are agglomerates of nanocrystals. Li et al. (2010) reported that using $Na_2S \cdot 9H_2O$ as sulfur source has better yield (84.8%) at 150℃ synthesis for 24 h.

Dixit et al. (1998) reported that thiourea (sulfur source) plays an important role not only in precipitating the particles but also in controlling the size and stability of the particles. In the case of the Nonyl phenyl ether (NP-30, non-ionic surfactant), the thiourea stabilizes the particles. When the cetyltrimethylammonium bromide (CTAB, cationic surfactant) is used, thiourea does not offer as much stability, whereas when the Sodium dodecylbenzenesulfonate (SDBS, anionic surfactant) is employed, instead of stabilizing the particles the thiourea is responsible for precipitating the particles. They also concluded the basic role for surfactants in the synthesis of nanoparticles arises out of its ability for compartmentalization. Darouie et al. (2013) reported that cetyltrimethylammonium bromide (CTAB, cationic surfactant) has better yield (82%) of CuS than sodium dodecyl sulfate (SDS, anionic surfactant) (76%).

For time and temperature:

Tanveer et al. (2014) used solvothermal method ($Cu(NO_3)_2 \cdot 3H_2O$, sulfur powder, Cu to S molar ratio = 1: 2) sythesis CuS at 140 ℃ to 160 ℃, 180 ℃,

and 200 ℃ for 8 h, 12 h, and 24 h. In case of sythesis at 180 ℃ for various time, 8 h get single wall cuboctahedra (SWCO) has specific surface area = 16 m^2/g, 12 h get double wall cuboctahedra (DWCO) has specific surface area = 24 m^2/g, 24 h get super complex cuboctahedra (SCCO) has specific surface area = 41 m^2/g. They reported that the more complex hierarchical structures (high specific surface area) were obtained with increased synthesis reaction times and temperature, the schematic for CuS growth mechanism show on Fig. 2-2.

The CuS particle size has been decreased for increasing reaction time (Suja et al., 2013). The form of CuS particles will change to plates (hierarchical structures) with increasing reaction temperature (Yan et al., 2013).

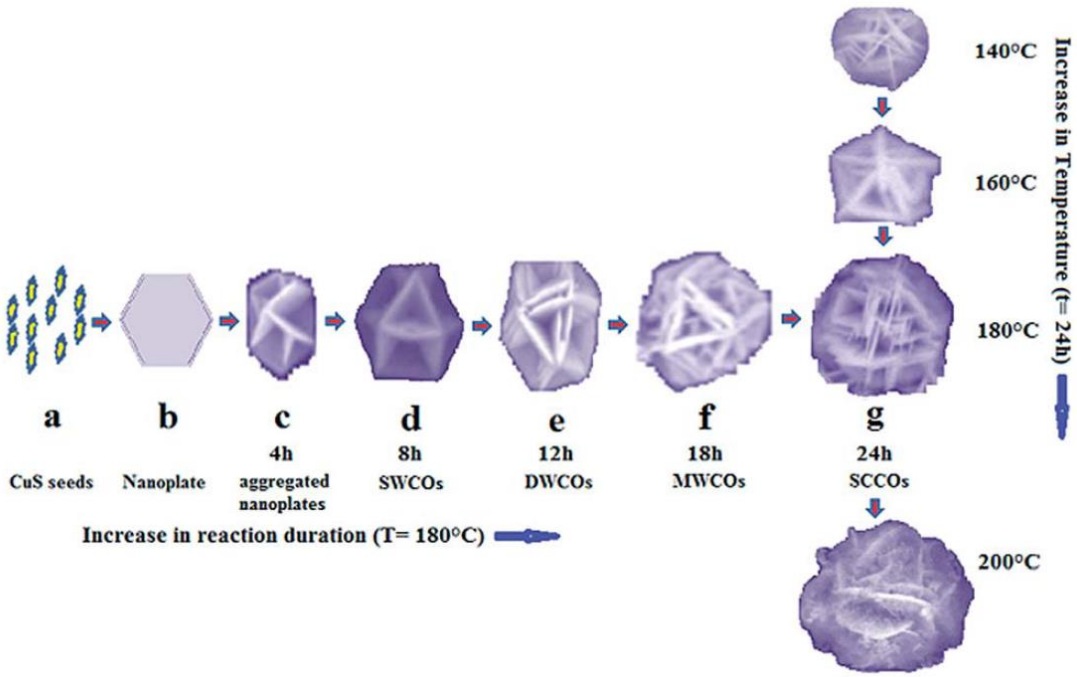

Fig. 2-2 Growth mechanism for the CuS. (SWCO, single wall cuboctahedra), (DWCO, double wall cuboctahedra), (MWCO, multiwall cuboctahedra) (SCCO, super complex cuboctahedra) (Tanveer et al., 2014)

In comparison with hydrothermal and solvothermal method, hydrothermal route is a simpler, low cost, environment friendly because it just need water as solvent instead of chemical solvent needed in solvothermal route. In addition, the elements S and Cu in the copper chalcogenides are “liquidus” so as to fabricate other materials without destruction of morphology (Zhuang et al., 2012). The reaction can be defined as a method of synthesis of single crystals that depends on the solubility of minerals in hot water under high pressure. The crystal growth is performed in an apparatus consisting of a steel pressure vessel called an autoclave, in which a nutrient is supplied along with water. A temperature gradient is maintained between the opposite ends of the growth chamber. At the hotter end the copper salt and sulfate salt solute dissolves, while at the cooler end it is deposited on a seed crystal, growing the desired crystal (Shamraiz et al., 2016).

In our study, we used copper chloride dihydrate ($CuCl_2 \cdot 2H_2O$) as copper source, sodium sulfide nonahydrate ($Na_2S \cdot 9H_2O$) as sulfur source, and cetyltrimethyl ammonium bromide (CTAB, $C_{19}H_{42}NBr$) as cationic surfactant to synthesis CuS crystals via hydrothermal method. To investigate the factors affecting the morphology, the molar ratios of copper (Cu) to sulfur (S) was 1:6, 1:8 and 1:10. To synthesis for 24, 48 and 72 h and reaction temperature fixed at 130℃ which is the median from review range (60–300℃).

Table 2-1-1 Studies of Copper monosulfide (CuS, Covellite) synthesis.

Methodology / Copper source (Cu)/ Sulfur source (S)/ Surfactant(SF)	Morphology	Energy band-gap (eV)	Results	Ref.
Spray pyrolysis deposition Cu: $CuCl_2 \cdot 2H_2O$, 0.016 M S: $SC(NH_2)_2$, 0.08 M (Cu:S = 1:5) SF: Cetylpyrydinium bromide (cationic), 1.67×10^{-2} wt%	Films: 15–48 nm (thickness)	2.2	–	(Naşcu et al., 1997)
Cu: $Cu(CH_3COO)_2 \cdot H_2O$ S: $SC(NH_2)_2$ SF1: Sodium dodecylbenzenesulfonate (anionic) SF2: Cetyltrimethylammonium bromide (cationic) SF3: Nonyl phenyl ether (non-ionic)	–	–	1. The basic role for surfactants in the synthesis of nanoparticles arises out of its ability for compartmentalization. 2. Thiourea plays an important role not only in precipitating the particles but also in controlling the size and stability of the particles. In the case of the NP-30, the thiourea stabilizes the particles. When the CTAB is used, thiourea does not offer as much stability, whereas when the SDBS is employed, instead of stabilizing the particles the thiourea is responsible for precipitating the particles.	(Dixit et al., 1998)
Silica-based sol-gel Cu: $Cu(NO_3)_2$ S: H_2S	Particles: 10–50 nm	2.3	–	(Gurin et al., 2003)
Solution (ion exchanging) Cu: $Cu(CH_3COO)_2 \cdot H_2O$, 2.5 mM S: CH_3CSNH_2, 2.5 mM (Cu:S = 1:1) SF: sodium-bis(2-ethylhexyl) sulfosuccinate (anionic), 0.05 mM and 0.5 mM	Particles: 20–60 nm (Without SF), 10–30 nm (0.05 mM SF), 10 nm (0.5 mM SF)	–	The particle size of CuS decreases with the surfactant concentration.	(Simonescu et al., 2008)
Hydrothermal (180 ℃ for 24 h) Cu: $CuCl_2 \cdot 2H_2O$, 0.1 M S: $Na_2S \cdot 9H_2O$, 03 M (Cu:S = 1:3) SF: Cetyltrimethylammonium bromide (cationic)	Plates: 15–60 nm	–	–	(Zhang and Zhang, 2008)
Chemical precipitation (50 ℃ for 2h) Cu: $CuCl_2 \cdot 2H_2O$, 0.05 M S: $SC(NH_2)_2$, 0.065 M (Cu:S = 1:1.3)	Particles:	2.25	–	(Pop et al., 2011)
Successive Ionic Layer Adsorption and Reaction Cu: $CuCl_2 \cdot 2H_2O$ S: $Na_2S \cdot 9H_2O$	Films: 28.1nm (thickness)	2.15	–	(Awodugba and Ibiyemi, 2012)

Table 2-1-2 Studies of Copper monosulfide (CuS, Covellite) synthesis

Methodology / Copper source (Cu)/ Sulfur source (S)/ Surfactant(SF)	Morphology	Energy band-gap (eV)	Results	Ref.
Hydrothermal (80 ˚C for 24 h) Cu: $Cu(CH_3COO)_2 \cdot H_2O$, 1.5 mM S: CH_3CSNH_2, 3 mM (Cu:S = 1:2) SF1: CTAB(cationic surfactant), 2.1 mM SF2: SDS (anionic surfactant), 2.1 mM	Particles: 16–23 nm	–	CTAB (82%) was better than SDS (76%) for yield %.	(Darouie et al., 2013)
Solvothermal (125 ℃ for 10 h, 15 h, 20 h) Cu: $Cu(NO_3)_2 \cdot 3H_2O$, 1mM S: $SC(NH_2)_2$, 2 mM (Cu:S = 1:2)	Particles: 35 nm (10 h), 27 nm (15 h), 24 nm (20 h)	–	The particle size has been decreased for increasing reaction time.	(Suja et al., 2013)
Microwave- hydrothermal (100,150, 200 ℃ for 4 h then 100,150 ˚C for 15 to 45 min using 300W of microwave power) Cu: $Cu(NO_3)_2$, 5 mM S: CH_3CSNH_2, 5 mM (Cu:S = 1:1) SF: polyvinylpyrrolidone	Particles: (100˚C) 20–70 nm Plates: (150, 200 ˚C) 5–10 nm (thickness)	1.8	The form of CuS particles will change to plates (hierarchical structures) with increasing reaction temperature.	(Yan et al., 2013)
Solvothermal (180 ℃ for 20 h) Cu: $Cu(CH_3COO)_2 \cdot H_2O$, 0.1M S: $SC(NH_2)_2$, 0.3M (Cu:S = 1:3) SF: poly (ethane 1,2-diol)-400 (Nonionic surfactant)	Plates: 50–120 nm (size), 10–30 nm (thickness)	2.26	–	(Rajendran and Gajendiran, 2015)

2.2.2 **Photocatalytic Activity of CuS**

CuS applied in photocatalysis often combine with Fenton-like reactions (adding H_2O_2), due to this process can overcome the drawback of charge recombination then enhance the photodegradation rate of organic pollutants and it is free from iron ions, leading to the separation of reactants from ions to solid materials. There have many studies using CuS and hydrogen peroxide (H_2O_2) for degrading organic compounds list systematically and shown in Table 2-2. Li et al. (2016) reported the Rhodamine B (RhB, 10 mg/L, 250 mL) degradation efficiency of CuS (0.1 g) with adding H_2O_2 (2mL) was higher than without adding H_2O_2 under visible light. (95% of RhB was degraded by CuS with H_2O_2 and 60% of RhB was degraded by CuS without H_2O_2 after 30 min.) The degradation of organic dye molecules in the CuS introduced Fenton-like reactions can be proceed efficiently without the adjustment of pH value (Xu et al., 2015). These advantages make the CuS introduced Fenton-like reactions more cost efficient by avoiding the ion removal and pH rectification.

Moreover, CuS is one of the excellent photocatalysts for degradation of organic dye (as shown in Table 2-2), but just few studies degraded other organic contaminants. Such as Saranya et al. (2015) synthesized CuS by hydrothermal route and reported that nitrobenzene and 4-nitrophenol were completely degraded after 60 min. So in our study, herbicide “paraquat” would be investigated utilize CuS as photocatalyst.

Table 2-2-1 Photocatalysis studies of CuS (Covellite)

Methodology / Copper source (Cu)/ Sulfur source (S)/ Surfactant(SF)	Morphology	Energy band-gap (eV)	Results/Catalytic Activity (Methylene blue (MB)/Rhodamine B (RhB)/ Methyl Orange (MO)/Bromocresol Green (BCG))	Ref.
Solvothermal (90 ℃ to 120 ℃, 150 ℃, and 180 ℃ for 4 h, 8 h, 12 h, and 24 h) Cu: $Cu(NO_3)_2 \cdot 3H_2O$ S1: $Na_2S \cdot 9H_2O$ S2: CH_3CSNH_2 S3: $SC(NH_2)_2$ (Cu:S = 1:2)	Plates: 10–40 m (thickness)	–	1.CuS microspheres composed of nanoplates or nanorods start to form at the early stage (4 h). As time develops (8 h and 12 h), CuS microspheres aggregate with each other to form hierarchical structures. 2.At 90 ℃, all microspheres are made up of densely packed nanoplates with very thin thickness in the range from 10 to 20 nm. At 120 ℃, all microspheres consist of sparsely packed nanoplateswith the thickness in the range from 30 to 40 nm. 3. It has better yield (84.8%) using $Na_2S \cdot 9H_2O$ at 150℃ for 24h. 4. CuS (30 mg), MB (20 mg/ L, 40 mL), H_2O_2 (1.3 mL, 30%, w/w) under the natural light. About 90% of MB was degraded after 90 min.	(Li et al., 2010)
Hydrothermal (180°C for 36 h) Cu: $CuCl_2$, 0.045 M S: Na_2S,0.3 M (Cu:S = 1:2) SF: CTAB,0.0082 M	Particles: 50–70 nm	2.35	CuS (0.5 g/L), MB (100 mg/ L), pH 6.0 at 30 ± 1◦C under solar light. About 70% of MB was degraded after 60 min.	(Gupta et al., 2012)
Solvothermal (160°C for 8 h, 12 h, 16 h, 24 h) Cu: copper foam S: sulfur powder (Cu:S = 1:1)	Hierarchical particles: 20–25 μm	–	1.At 8 h, consists of many cubic crystals with a diameter distribution of 10–20 μm. When the reaction time increased to 12 h, the cubic crystals in 8 h changed into 3D hierarchical architectures, with a diameter distribution of 4–11 μm and thickness of each flake of 1 μm. When the reaction time was 16 h, the flakes on the hierarchical architectures gradually grew thinner (to about 100 nm). 2.CuS (0.05 g), MB (5 mg/L), H2O2 (10 mL). 95% of MB was degraded after 20 min.	(Li et al., 2012)

Table 2-2-2 Photocatalysis studies of CuS (Covellite)

Methodology / Copper source (Cu)/ Sulfur source (S)/ Surfactant(SF)	Morphology	Energy band-gap (eV)	Results/Catalytic Activity (Methylene blue (MB)/Rhodamine B (RhB)/ Methyl Orange (MO)/Bromocresol Green (BCG))	Ref.
Solvothermal (60 ˚C for 16 h) Cu: copper foam S: sulfur powder (Cu:S = 1:1)	Ball-flower: 20–35 μm	–	CuS (0.05 g), MB (10 mg/ L, 30 mL), H_2O_2 (10 mL) at 30˚C under UV lamp. 96% of MB was degraded after 25 min.	(Mi et al., 2013)
Solution (ion exchanging) Cu: $Cu(NO_3)_2 \cdot 3H_2O$, 0.3 M S: Na_2S, 1 M	Particles	3.1	CuS (0.1 g/L), BCG and MO (10 mg/ L, 20 mL) under solar light 1. Decolorization efficiency of various photocatalysts was CuS > ZnO > FeO > CdS > NiS > ZnS > CdO > NiO > FeS. 2. 32% of MO was degraded after 480 min. 3. 58% of BCG was degraded after 480 min.	(Nezamzadeh-Ejhieh and Moazzeni, 2013)
Ultrasonic Cu: $Cu(CH_3COO)_2 \cdot H_2O$, 1 mM S: $SC(NH_2)_2$, 4 mM (Cu:S = 1:4)	Hollow sphere: 200–500 nm, 25.4 m^2/g	1.27	CuS (20 mg), MB and RhB (50mg /L, 20mL) H_2O_2 (0.5 mL) 1. 95.6% of MB was degraded after 30 min. 2. 90.7% of RhB was degraded after 40 min.	(Deng et al., 2014)
Solvothermal (150 ˚C for 24 h) Cu: $CuSO_4 \cdot 5H_2O$, 1 mM S: $SC(NH_2)_2$, 2 mM (Cu:S = 1:2)	Spheres: 10–16 nm, 23 m^2/g	3.38	CuS (30 mg/L), MB (1.6 mg/L), pH 8.0 under visible light. 25% of MB was degraded after 40 min.	(Sohrabnezhad et al., 2014)
Hydrothermal (150˚C for 24 h) Cu: $Cu(NO_3)_2 \cdot 3H_2O$, 1 mM S: $SC(NH_2)_2$, 2.5 mM SF: CTAB, 0.2 mM (Cu:S = 1: 2.5)	Plates: 40–80nm	1.87	CuS (30 mg), MB (20 mg/ L, 40 mL) under visible light. 87% of MB was degraded after 40 min.	(Saranya et al., 2014a)

Table 2-2-3 Photocatalysis studies of CuS (Covellite)

Methodology / Copper source (Cu)/ Sulfur source (S)/ Surfactant(SF)	Morphology	Energy band-gap (eV)	Results/Catalytic Activity (Methylene blue (MB)/Rhodamine B (RhB)/ Methyl Orange (MO)/Bromocresol Green (BCG))	Ref.
Hydro/solvothermal (70˚C for 4 h) Cu1: $Cu(NO_3)_2$, Cu2: $CuCl_2$ Cu3: $CuSO_4$ Cu4: $Cu(OAc)_2$ S: $Na_2S_2O_3$, ($Cu(NO_3)_2$:$Na_2S_2O_3$ = 1:1, 1:2, 2:1)	Spheres: 400-500 nm, Tubes: 8–10 μm (L) 0.5–10 μm (D), Plates: 50–100 nm, Particles: 10–25 nm	Spheres: 2.08, Tubes: 2.06, Plates: 2.16, Particles: 1.88	1. With increases in the reaction temperature from 70 to 180 ℃, the length of nanotubes remains same (~1 μm) whereas the average diameter is found to be increased to ~400 nm (at 120 ℃) and ~500 nm (at 180 ℃) from 200 nm (at 70 ℃) 2. With a 1:1 molar ratio of $Cu(NO_3)_2$ and $Na_2S_2O_3$, only CuS nanotubes was obtained. With a 2:1 molar ratio of $Cu(NO_3)_2$ and $Na_2S_2O_3$, both CuS nanotubes and nanoparticles were obtained. With a 1:2 $Cu(NO_3)_2$ and $Na_2S_2O_3$ molar ratio, there were no CuS nanotubes or other nanostructures. 3. The diameter of CuS nanotubes formed in the presence of $CuSO_4$ (~400 nm) is found to be larger than that obtained with $Cu(NO_3)_2$ (<200 nm). With $CuCl_2$ and $Na_2S_2O_3$, no nanotubes were obtained. The structures obtained with $CuCl_2$ and $Na_2S_2O_3$ precursors are the agglomeration of nanoflakes with a thickness <25 nm. With $Cu(OAc)_2$ and $Na_2S_2O_3$, CuS nanoparticles are formed instead of nanotubes or nanoflakes 4. CuS (30 mg), MB (20 mg/ L, 40 mL), H_2O_2 (1 mL) at 30˚C MB degradation for 25min in the dark. Spheres: 97%, Tubes: 94%, Plates: 95%, Particles: 97%. 5. A slightly higher MB degradation (~2−3 %) was found initially in the presence of light as compared to dark and becomes almost equal after 15 min.	(Kundu and Pradhan, 2014)

Table 2-2-4 Photocatalysis studies of CuS (Covellite)

Methodology / Copper source (Cu)/ Sulfur source (S)/ Surfactant(SF)	Morphology	Energy band-gap (eV)	Results/Catalytic Activity (Methylene blue (MB)/Rhodamine B (RhB)/ Methyl Orange (MO)/Bromocresol Green (BCG))	Ref.
Solvothermal (140 ℃ to 160 ℃, 180 ℃, and 200 ℃ for 8 h, 12 h, and 24 h) Cu: $Cu(NO_3)_2 \cdot 3H_2O$, 1 mM S: sulfur powder, 2 mM (Cu:S = 1: 2)	Hierarchical particles, 400-500 nm SWCO (8 h): 16 m^2/g, DWCO(12 h): 24 m^2/g, SCCO(24 h): 41 m^2/g	SWCO: 1.70, DWCO: 1.86, SCCO: 1.96	1. The more complex hierarchical structures (high specific surface area) were obtained with increased synthesis reaction times and temperature. 2. CuS (20 mg), MB (1.6 mg/L) H_2O_2 (1 mL) at room temp. MB degradation within 50min under natural light. SWCO: 60%, DWCO: 72%, SCCO: 96%	(Tanveer et al., 2014)
Hydrothermal (Cu:S=1:1, 1:2, 1:4 for 60℃, 10 min；Cu:S=1:4 for 30℃, 40℃, 60℃, 90℃, 10 min; Cu:S=1:4 for 60℃, 10 min, 30 min, 60 min, 300 min) Cu: $Cu(NO_3)_2 \cdot 3H_2O$ S: CH_3CSNH_2	Particles: 20–50 nm	–	1. Extending the growing time and temperature led to CuS particles of increased size. 2. Changing the Cu:S molar ratio did not affect the crystallinity of the obtained products. Varying the Cu:S molar ratio from 1:1, 1:2 to 1:4 gradually transforms particles from a nanoplate shape with broad size distribution to more well defined nanoplates and then to spherical nanoparticles of size 20–50 nm. In addition the particle size distribution narrows as the S content is increased, due to CH_3CSNH_2 influencing both CuS nanocrystal nucleation and growth process, by initiating CuS nanocrystals formation and also acting as a surfactant to influence the reaction kinetics. Hence at high Cu:S ratios (Cu-rich) TAA acts only as the sulfur precursor forming CuS particle with non-uniform size. The fact crystallite size from XRD is invariant of Cu:S ratio suggests these particles are agglomerates of nanocrystals. 3. CuS (1 mg), RhB (1×10^{-5} M, 1.0 mL) under visible light. 23% of RhB was degraded after 30 min.	(Thuy et al., 2014)
Chemical dealloying (90°C for 48 h) Cu: copper powder S: Sulfuric acid	Particles: 50–100 nm, 4.3–28.7 m^2/g	1.6–1.7	CuS (10 mg), MB (10 mg/L or 1000 mg/L, 6.0 mL), H_2O_2 (2mL) under 500 W Xe lamp with 0.01 W/cm irradiance. 1. 10 mg/L MB solution was degraded completely in 40 s. 2. 98% of 1000 mg/L MB was degeneratied within 16 minutes. 3. The Cu^+ can react with H_2O_2 to generate hydroxyl radicals and further improve the photocatalytic property.	(Xu et al., 2015)

Table 2-2-5 Photocatalysis studies of CuS (Covellite)

Methodology / Copper source (Cu)/ Sulfur source (S)/ Surfactant(SF)	Morphology	Energy band-gap (eV)	Results/Catalytic Activity (Methylene blue (MB)/Rhodamine B (RhB)/ Methyl Orange (MO)/Bromocresol Green (BCG))	Ref.
Solvothermal (150°C for 24 h) Cu: $Cu(NO_3)_2 \cdot 3H_2O$, 1 mM S1: $Na_2S \cdot 9H_2O$, 2.5 mM S2: $SC(NH_2)_2$, 2.5 mM (Cu:S = 1: 2.5)	Plates: 40–110 nm	2.08	1. The morphology was not well-defined and uniform in the case of $Na_2S \cdot 9H_2O$ as sulfur source. This could be due to the week coordination of $Na_2S \cdot 9H_2O$ with Cu in CuS nanostructures. When $Na_2S \cdot 9H_2O$ was used, the products were grown in an isotropic mode and their final morphology was small nanoparticles.When $SC(NH_2)_2$ were used, anisotropic growth played a vital role in the synthesis of metal sulfide nanocrystals, accordingly, the final products were nanorods, nanoplates or their assemblies. 2. 4-nitrophenol were completely degraded after 60 min.	(Saranya et al., 2015)
Solvothermal (170°C for 5 h) Cu: $CuCl_2 \cdot 2H_2O$, 0.02 M S: $SC(NH_2)_2$, 0.08 M (Cu:S = 1: 4)	Ball-flower: 1–5μm	1.45	CuS (0.025 g, 0.05 g and 0.1 g), MB (0.5 g/L, 50 mL) under UV or visible light irradiation. 1. Degradation rate increased with CuS dosage. 2. For 0.1 g CuS, 69.5% of MB was degraded after 15min under UV light. 89.3% of MB was degraded after 15 min under visible light.	(Hu et al., 2016)
Mechanochemical ball milling Cu: copper powder S: sulfur powder (Cu:S = 1:1)	Particles: (Quantum dots, QDs) <5 nm, 90.0 m^2/g ; Plates (NPs) 13.1m^2/g	QDs: 1.87 NPs: 2.27	CuS (0.1 g), RhB (10 mg/L, 250 mL), H_2O_2 (2mL) under visible light. 1. 95% of RhB was degraded by QDs with H_2O_2 after 30 min. 2. 60% of RhB was degraded QDs without H_2O_2 after 30 min. 3. 40% of RhB was degraded by NPs with H_2O_2 after 30 min.	(Li et al., 2016)

2.3 Paraquat

2.3.1 Properties and Hazards of Paraquat

Paraquat (1,1'-Dimethyl-4,4'-bipyridinium dichloride) is a quick acting and non-selective contact herbicide. It is one of the most extensively used herbicide in agricultural countries for the control of broad-leaved weeds and grasses in crop land and aquatic area due to its physical properties, such as high solubility in water, low vapor pressure, etc. The chemical structure of paraquat is shown in Fig. 2-3, and the properties of paraquat are shown in Table 2-3.

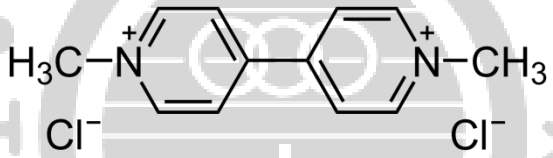

Fig. 2-3 Chemical Structure of Paraquat

Table 2-3 Properties and Hazards of Paraquat

Properties	
Molecular formula	$C_{12}H_{14}C_{l2}N_2$
IUPAC name	1,1'-Dimethyl-4,4'-bipyridinium dichloride
CAS number	1910-42-5
Molecular weight	257.16 g/mol
Physical state	White to yellow powder
Odor	Faint, ammonia-like
Density	1.25 g/cm^3
Melting point	175 to 180℃ (347 to 356℉)
Boiling point	> 300 ℃ (572℉)

Solubility in water at 25℃	0.7 g/cm^3
Vapor pressure	< 0.0000001 mmHg (20℃)
Hazards	
Main hazards	Toxic, environmental hazard
GHS pictograms	
LD_{50}	57 mg/kg (rat, oral) 120 mg/kg (mouse, oral) 25 mg/kg (dog, oral)
LC_{50}	3 mg/m^3 (mouse, 30 min respirable dust) 3 mg/m^3 (guinea pig, 30 min respirable dust)

2.3.2 Environmental Impact and Treatment

As herbicide, paraquat has been available to farmers for over 50 years. This chemical compound is adsorbed very fast on the leaves of any plant and inhibits the photosynthesis process (Slade and Calderblank, 1975). Paraquat is also persistent in soil due to its very strong sorption to clay particles and becomes inactive. It is less (and usually much less) than 0.1% of applied paraquat will be present in the interstitial water (Bromilow, 2004). In this form, paraquat does not represent any risk of fresh or waste water contamination. However, paraquat rinsate solutions produced during the fabrication, dilution, mixing, transfer and application of commercial pesticides may pollute the waste water lines and may reach the sources of fresh water (Somich et al., 1990). It is present as an environmental pollutant both in soil and in surface waters, which produces toxicity in human and animals. The minimum lethal dose of paraquat is stated to be about 35 mg/kg body weight for human beings (Bismuth et al., 1987).

Many efforts have been made to remove paraquat from the environment. The treatments to degrade contaminated paraquat in water are categorized as physical, biological and chemical routes. Physical adsorption onto diatomaceous earth, clays (Tsai et al., 2005) or carbon filters (Hamadi et al., 2004) requires further treatment. Most of the times, filters are sent to a land disposal facility. In some physical processes there is a simple transfer of the pollutants from one phase to another, not being destroyed; Microbial degradation processes are very slow and required long incubation times. In the case of high concentration of organic priority pollutants, the activated sludge formation can be substantially intoxicated and suppressed and waste sludge also needs further treatment (Lee et al., 1995; Singh and Singh, 2016); For chemical treatments of paraquat, the most widely applied treatment are advanced oxidation processes (AOPs) due to their powerful capability to oxidize numerous organic compounds into small pollution-free compounds, CO_2 and H_2O (Glaze et al., 1987). These are clean technologies based on the generation of extremely reactive and non-selective hydroxyl radicals ($^{\bullet}OH$). Hydroxyl radicals are produced with the help of one or more primary oxidants (e.g. ozone, hydrogen peroxide and oxygen), energy sources (e.g. ultraviolet light) or catalysts (e.g. titanium dioxide). Andreozzi et al., (1993) degraded 231–2057 mg/L paraquat at pH4.2–8.0 via ozonation. Cartaxo et al., (2015) reported that the electrode pair Pt/steel was used for the electrochemical oxidation of 10^{-4} M paraquat reached removal 79% after 1.5 h of electrolysis. Santos et al. (2011) used Fenton's reagent to degrade paraquat (100 mg/L) and about 40% of mineralization were reached after 4 h of reaction (batch

reactor).

Paraquat can also be degraded by photocatalytic processes, in which photoinduced holes in semiconductor particles oxidize hydroxide ions or water molecules adsorbed on the surface of the particles to produce $^{\bullet}OH$ and $^{\bullet}O_2^-$ radicals which subsequently attack adsorbed organic molecules. Cantavenera *et al*., (2007) used 0.4 g/L Degussa P25 TiO_2 for degradation of paraquat (20 mg/L) under ultraviolet (UV) light, an almost complete removal of paraquat was achieved after approximately 3 hrs and Moctezuma *et al*. (1999) reported that the degradation of paraquat (20 and 40 mg/L) with 2.0 g/L Degussa P25 TiO_2 under UV light at high pH values increased the initial rate of photocatalytic reaction and destroyed 60% of contaminant in less than 3 hrs of reaction. However, those techniques are limited by UV radiation which is inconvenient to obtain in nature.

In Fenton's reagent treatment, owing to the necessary high dosage of iron and hydrogen peroxide, to achieve a high mineralization yield of the pollutant, as well as the continuous loss of catalyst and the important amount of generated iron hydroxide sludge, needs further separation. One of the most practical and interesting ways proposed to circumvent these limitations is the use of heterogeneous Fenton-like oxidation. Some studies degraded paraquat also via this route. Dhaouadi and Adhoum (2010) used iron-modified activated carbon (AC-Fe) as catalyst and added hydrogen peroxide (H_2O_2) to remove 20 mg/L paraquat solution. The best degradation yield (71.4% of COD abatement in a 20 mg/L solution) was obtained with 12.5 mmol/L H_2O_2, 1.0 g/L catalyst dosage at 70 ^{o}C. Miguel et al. (2012) reported added H_2O_2 would enhance the

photocatalytic reaction, the results of photocatalytic treatment with 1.0 g/L of Degussa P25 TiO_2 under UV/VIS radiation during 30 min achieves an average degradation of the studied pesticides of 48%. After added 10 mM H_2O_2, the average degradation of pesticides increased up to 57%.

In summary, the TiO_2 semiconductor has undoubtedly proven to be one of the excellent photocatalysts for degradation of herbicide “paraquat”. However, due to its wide band-gap of 3.2 eV, TiO_2 can only be excited by ultraviolet or near-ultraviolet radiation, which occupies only 4% of the incoming solar light spectrum on the earth (Chen et al., 2010). To efficiently utilize the visible region ($\lambda > 400$ nm) which covers the largest proportion of the solar spectrum, the development of visible-light-driven (VLD) photocatalysts is the current trend. Moreover, CuS is one of the excellent photocatalysts for degradation of organic dye (Table 2-2), but just few studies degraded other organic contaminants. Such as Saranya et al. (2015) synthesized CuS by hydrothermal route and reported that nitrobenzene and 4-nitrophenol were completely degraded after 60 min.

There are no more studies about degradation of paraquat using CuS as photocatalyst in the past. Hence, we were focus on CuS as photocatalyst to degrade paraquat via heterogeneous photo-Fenton-like oxidation under visible light.

Chapter 3 Methodology

The methodology was divided into two parts. The study chart was shown in Fig. 3-1. The first part was preparation of copper sulfide (CuS) nanocrystals by using hydrothermal method, and characterizations were examined by X-Ray diffraction, scanning electron microscope and UV-Vis diffuse reflectance spectroscopy. The second part was utilizing CuS as photocatalyst to degrade paraquat under visible light for the environmental applications. Furthermore, the photocatalytic activity, kinetic and mechanism of CuS nanocrystals were evolved by Langmuir–Hinshelwood (L–H) model.

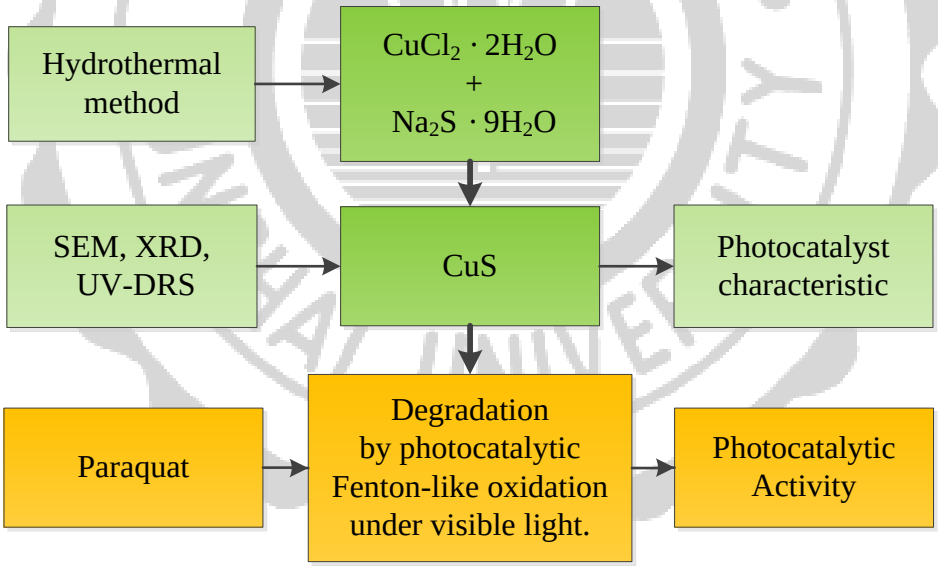

Fig. 3-1 Study chart for hydrothermal synthesis of CuS as photocatalyst to degrade Paraquat via heterogeneous photo-Fenton-like oxidation under visible light.

3.1 Materials and Apparatus

3.1.1 Chemicals

1. Copper chloride dihydrate ($CuCl_2 \cdot 2H_2O$, ≥98%, Carlo Erba, France) as copper source of CuS.
2. Sodium sulfide nonahydrate ($Na_2S \cdot 9H_2O$, ≥99.9%, Carlo Erba, France) as sulfur source of CuS.
3. Cetyltrimethyl ammonium bromide (CTAB, $C_{19}H_{42}NBr$, ≥99%, Acros Organics, U.S.A.) as cationic surfactant in the formation of nanoparticles is due to the compartmentalization offered by host surfactant assemblies (Dixit et al., 1998).
4. Ethanol (C_2H_6O, 95%, Sigma-Aldrich, Germany) as clean reagent of as-prepared materials.
5. Methyl viologen dichloride hydrate (Paraquat, $C_{12}H_{14}C_{l2}N_2 \cdot xH_2O$, ≥98%, Acros Organics, U.S.A.) as a pollutant probe of photocatalytic Fenton-like oxidation system.
6. Titanium dioxide P25 (TiO_2 P25, >99.5% Aeroxide, China) as commercial photocatalyst to compare with as-prepared materials.
7. Hydrogen peroxide (H_2O_2, 30% w/w in water, Carlo Erba, France) as an electron acceptor can enhance the photodegradation rate of organic pollutants due to overcomes the drawback of charge recombination (Kitsiou et al., 2009).

3.1.2 Apparatus and Instrument

1. Teflon-lined stainless steel autoclave (external diameter = 7.5 cm, height = 16.5 cm) as reactor of crystallization synthesis.
2. Oven (ED240, Binder, Germany) provided high-temperature ambience for hydrothermal synthesis process.
3. Compact centrifuge (Z206, Hermle Labortechnik, Germany) centrifuged the product solution of synthesis to separate the product and clean reagents (water and ethanol).
4. Pyrex glass photoreactor (250 mL) as reactor of photocatalytic Fenton-like oxidation system.
5. Magnetic stirrer (C-MAG HS 7, IKA, Germany) maintained the suspension of photocatalyst.
6. LED visible light bulb (6W, Philips, China) as radiation source of photocatalytic Fenton-like oxidation system.
7. Solarimeter (SL100, from Kimo, France) measured the light intensity of LED bulb.
8. UV meter (UV-meter 5.0, Solartech, USA) confirmed that the radiation was only in visible light range.
9. Refrigerated water bath circulator (RTE-111, Neslab, U.S.A.) kept the photoreactor at room temperature (25℃).
10. UV-Visible spectrophotometer (V-630, Jasco, Japan) analyzed paraquat concentration with a detector set at λ_{max} = 257 nm.
11. Laboratory glasswares

3.2 CuS Synthesis

In this study, copper sulfide (CuS) nanocrystals is the photocatalyst was prepared from copper chloride dehydrate ($CuCl_2 \cdot 2H_2O$) which provide copper source and sodium sulfide nonahydrate ($Na_2S \cdot 9H_2O$) as sulfur source. The synthesis method of copper sulfide (CuS) nanocrystals by hydrothermal method was modified from Zhang's method (Zhang and Zhang, 2008). The CuS samples synthesized with different molar ratios of copper-to-sulfur (1:6, 1:8 and 1:10) and synthesis times (24, 48 and 72 h) at 130℃. The synthesis procedures are listed consequently as follows (shown in Fig. 3-2):

1. Copper chloride dehydrate ($CuCl_2 \cdot 2H_2O$, 3 mmol) mixed with cetyl trimethyl ammonium bromide (CTAB, 1 mmol) in 60 ml of distilled water stirred for 10 min. CTAB was surfactant which can enhance the link between copper (Cu) and sulfur (S).
2. Sodium sulfide nonahydrate ($Na_2S \cdot 9H_2O$, 30 mmol) solution was poured into buret. Then drop by drop added in solution from previous step. The ratios of copper to sulfur in 120 ml of solutions were 1:6, 1:8 and 1:10.
3. After stirring 30 min, the mixture was transferred to Teflon-lined stainless steel autoclave for hydrothermal treatment.
4. Placing the autoclave in oven for 24, 48, 72 hrs at 130℃.
5. The precipitates were washed by distilled water and ethanol, centrifuged at 5000 rpm for 5 min and dried in vacuum oven at 60℃ for overnight.

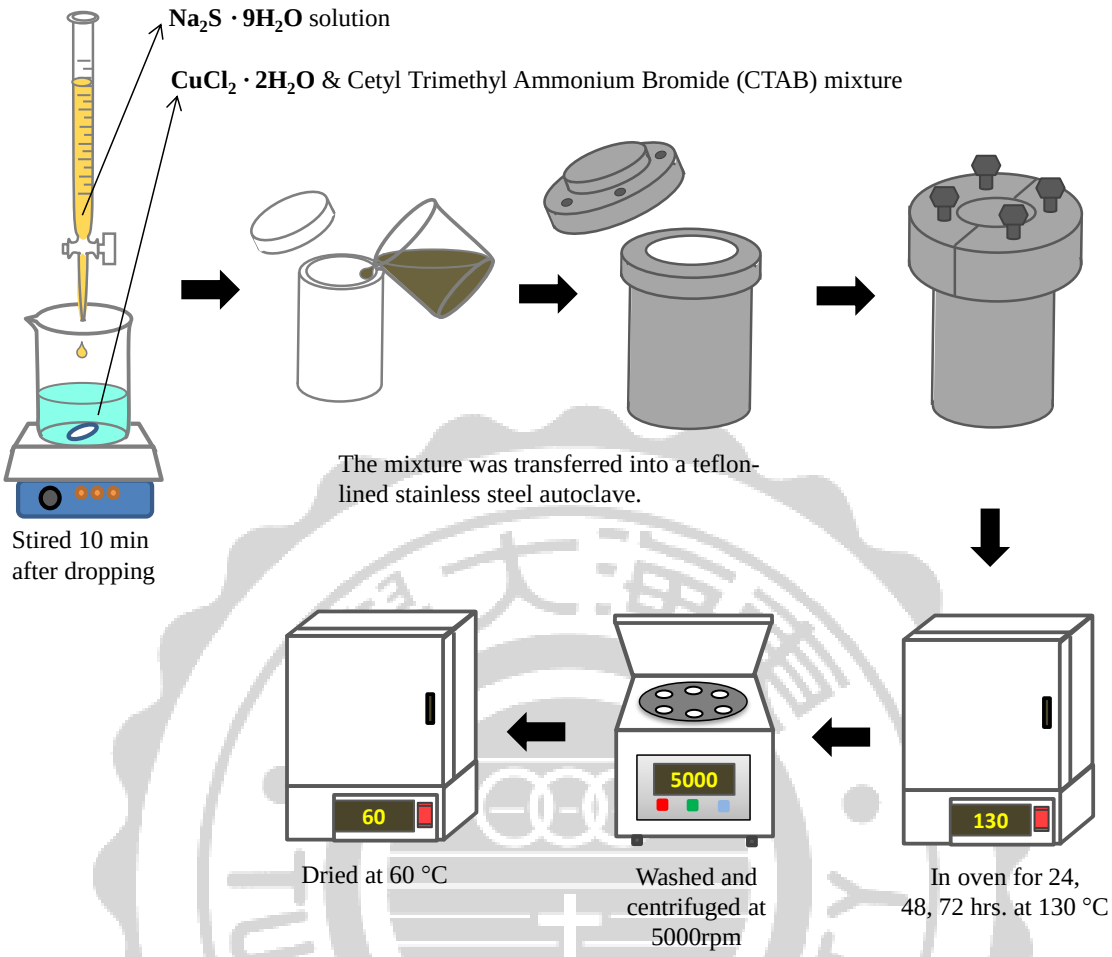

Fig. 3-2 Copper(II) sulfide (CuS) nanocrystals preparation

3.3 Materials Characterizations

The physical-chemical properties of synthesized CuS photocatalysts include distribution, length, diameter, crystal structure, microstructure and optical properties were examined by various techniques such as X-Ray diffraction, scanning electron microscope and UV-Vis diffuse reflectance spectroscopy.

3.3.1 X-Ray Diffraction

The X-ray diffraction is one of the primary techniques used to characterize solid-state material, and can provide valuable information about the crystalline

phase and average crystallite size. Parallel monochromatic X-ray beam are directed onto the samples. The X-rays are then diffracted from the crystal, and carry information about the electron distribution in the material (Fig. 3-3). The XRD patterns were obtained using CuKα radiation on Bruker AXS (Model D8 Discover, Germany) diffractometer. The X-ray was generated with a current of 40 mA and a potential of 40 kV. The CuS samples were scanned from 20 to 80 degrees (2θ) in steps of 0.02 degrees per second.

The average crystallite size (*D*) of catalyst was estimated using Scherrer equation:

$$D = \frac{k\lambda}{\beta \cos\theta} \qquad \text{(Eq. 3-1)}$$

where D = crystallite size (nm), k = crystallite shape factor (0.94), λ = X-ray wavelength for CuKα (0.15406 nm), β = the full-width-half-maximum (FWHM) of the peak, θ = Bragg angle.

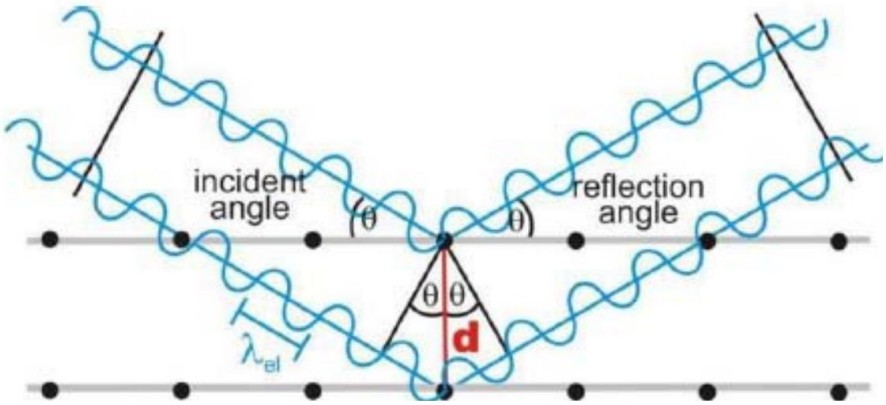

Fig. 3-3 Schematic diagram illustrating the constructive interference of scattered waves on sample

3.3.2 **Scanning Electron Microscope**

SEM is the most commonly used technique for this study to provide high-resolution images of nanostructure, with the advantages of high magnification, minimum sample preparation, and ease of observation and control. SEM uses a focused beam of high-energy electrons to generate a variety of signals at the surface of solid specimens. The signals that derive from electron-sample interactions reveal information about the sample including external morphology (texture), chemical composition, and crystalline structure and orientation of materials making up the sample. The external morphologies of 9 CuS samples were observed with a SEM (JEOL JSM-6610LV, Japan) operating in high vacuum mode with secondary electron image conditions and the electron micrograph technique. The SEM operates at 1 kV to 30 kV with an ultimate resolution of 3 nm to 1.2 nm. The accelerating voltage ranges from 0.3 kV to 30 kV, and the magnification range runs from 5X to 300,000X.

3.3.3 **UV-Vis Diffuse Reflectance Spectroscopy**

The diffusion reflectance of CuS samples were measured by UV-diffuse reflectance absorption spectrometer (Hitachi model U-3501, Japan) equipped with integrating sphere. The reflectance of samples was detected in the 400-800 nm wavelength range. The pure power of $BaSO_4$ was used as a reference. The energy band-gap for the CuS nanocrystals has been estimated from the adsorption spectra using the Tauc's law (1968):

$$(\alpha h\nu)^2 = A\left(h\nu - E_g\right) \qquad \text{(Eq. 3-2)}$$

where α is the optical absorption coefficient, hν is the photon energy (eV), E_g is the energy band-gap (eV), A = an energy-independent constant.

3.4 Fenton-like Photocatalytic Degradation Studies

There are two stages in photocatalytic degradation studies. The first stage was comparison of photocatalytic performances of 9 CuS samples synthesized with different mole ratios of copper to sulfur (1:6, 1:8 and 1:10) and synthesis times (24, 48 and 72 h) were evaluated by the paraquat degradation efficiency. The second stage was selecting the CuS which has better photocatalytic performances. The photocatalytic activities of CuS were evaluated by degradation efficiency of different concentration paraquat. Then the photodegradation kinetic will be investigated. The experimental set up are shown in Fig. 3-4: 40 mg of photocatalyst (1.0 g/L) and hydrogen peroxide (0.22 M) was introduced into 40 ml of paraquat solution in a 250 ml Pyrex glass photoreactor, and maintain the photoreactor at 25℃ by refrigerated water bath circulator. The reactor was placed at the fixed distance of 20 cm from a 6W LED bulb where the irradiance is equal to 6 W/m^2 and was stirred at constant speed during the photoreaction process. The reactor and LED bulb were insulated by 1.0 m^2 opaque cabinet.

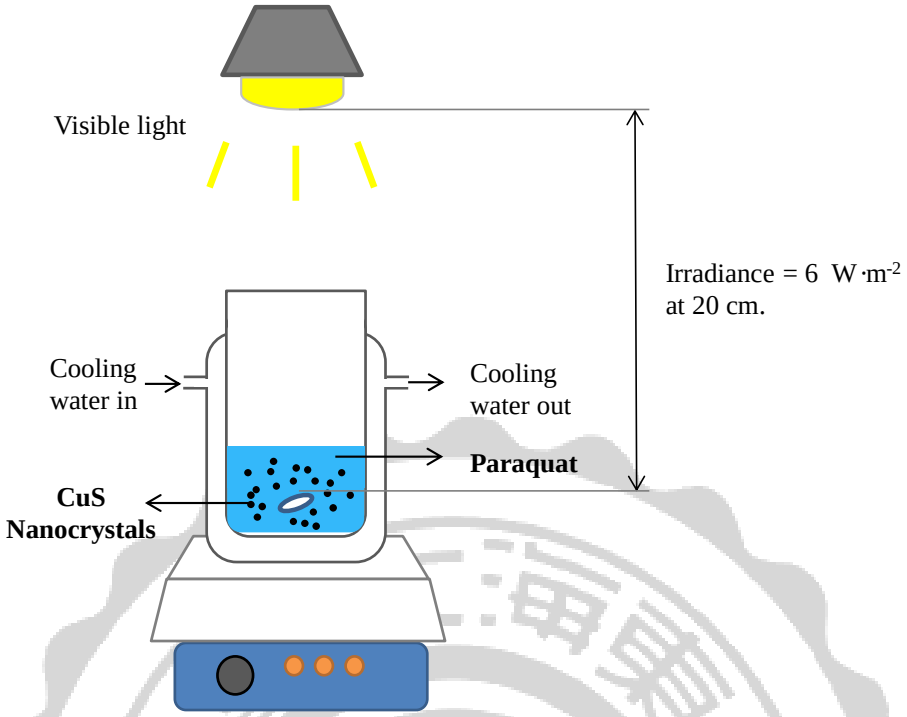

Fig. 3-4 The experimental set for photocatalytic degradation under visible light irradiation

3.4.1 Degradation of Paraquat with CuS by Various Synthesis Parameter

This stage was comparison of photocatalytic performances of CuS sample which were synthesized with different mole ratios of copper to sulfur (1:6, 1:8 and 1:10) and synthesis times (24, 48 and 72 h) at 130℃. They were evaluated by the paraquat degradation efficiency. The procedures are listed consequently as follows：

1. The initial concentration of paraquat was 40 mg/L throughout the photocatalytic reaction.
2. 40 mg of photocatalyst (1.0 g/L) was added into 40 ml of 40 mg/L paraquat solution.

3. The reaction mixture was magnetically stirred in the dark for 1 hr to establish adsorption equilibrium.
4. 1.0 mL of hydrogen peroxide (H_2O_2, 30% w/w in water) was added into the mixture. The first sample was taken out at the 10th minute after H_2O_2 was added.
5. The light was then turned on to initiate the reaction time, and sampling every 20 minutes.
6. The samples were collected and filtered with PTFE-Millipore disk (0.45 μm) to remove all photocatalysts.
7. The filtrates were analyzed by the Jasco V630 UV-Visible spectrophotometer at the characteristic band of 257 nm to determine the paraquat concentration.

3.4.2 Effect of Initial Paraquat Concentrations

This stage was choosing one of the CuS which has better photocatalytic performances from previous stage. The photocatalytic activities of CuS were evaluated by degradation efficiency of different concentration paraquat (20, 40, 60, 80, 100 mg/L). The procedures are listed consequently as follows：

1. 40 mg of photocatalyst (1.0 g/L) was added into 40 ml of paraquat solution (concentration = 20, 40, 60, 80, 100 mg/L).
2. The reaction mixture was magnetically stirred in the dark for 1 hr to establish adsorption equilibrium.
3. 1.0 mL of hydrogen peroxide (H_2O_2, 30% w/w in water) was added into

the mixture. The first sample was taken out at the 10th minute after H_2O_2 was added.

4. The light was then turned on to initiate the reaction time, and sampling every 10 minutes.
5. The samples were collected and filtered with PTFE-Millipore disk (0.45 μm) to remove all photocatalysts.
6. The filtrates were analyzed by the Jasco V630 UV-Visible spectrophotometer at the characteristic band of 257 nm to determine the paraquat concentration.

3.4.3 **Photocatalytic Activity and Kinetic**

Several kinetic models can be applied for the kinetic study of photocatalytic reaction, such as Langmuir-type, Quadratic-type and the direct–indirect (DI) kinetic model etc... Among them, Langmuir–Hinshelwood (L–H) model is the most commonly applicable for photoreaction of water dissolved organic compounds (Mills et al., 2015). Estimation of photodegradation rate was expressed by pseudo-first order (Eq. 3-3) in Langmuir-Hinshelwood kinetic model:

$$r = -\left(\frac{dC}{dt}\right) = k_{obs}C \qquad \text{(Eq. 3-3)}$$

where C is the concentration of paraquat (mM) at a given time. k_{obs} is the observed first-order rate constant.

From the integration of Eq. 3-3, the concentration–time equation will be derived in Eq. 3-4. A plot of $\ln(C_0/C_t)$ versus time leads to a linear diagram so that its slope equals the observed first-order rate (k_{obs}) constant of photodegradation.

$$\ln\left(\frac{C_0}{C_t}\right) = k_{obs}t \qquad \text{(Eq. 3-4)}$$

In this study, paraquat concentration is only one raw material of the photoreaction. The photocatalytic reaction is expressed as follows;

$$r = -\left(\frac{dC}{dt}\right) = \frac{k_r K_a C}{(1 + K_a C)} \qquad \text{(Eq. 3-5)}$$

where k_r is the surface reaction rate constant. K_a is the Langmuir–Hinshelwood adsorption equilibrium constant. C is the concentration of paraquat (mM) at a given time.

To evaluate those parameters, an initial rate method (Zhang et al., 2001) was applied. L–H rate expression (Eq. 3-5) could be written and linearized as follows;

$$r_0 = -\left(\frac{dC}{dt}\right) = \frac{k_r K_a C_0}{(1 + K_a C_0)} \qquad \text{(Eq. 3-6)}$$

$$\frac{1}{r_0} = \frac{1}{k_r K_a C_0} + \frac{1}{k_r} \qquad \text{(Eq. 3-7)}$$

Hence, the values of k_r and K_a can be estimated by plotting the reciprocal of degradation rate as a function of the reciprocal of initial parauat concentration.

Chapter 4 Results and Discussion

In this chapter, the synthesized CuS photocatalysts are characterized by several techniques including X-Ray diffraction, Scanning electron microscope and UV-Vis Diffuse Reflectance Spectroscopy. The photocatalytic activities (kinetic and mechanism) of paraquat degradation under visible light are reported as well.

4.1 Photocatalyst Characterization

The photocatalytic activities of the catalysts depend mainly upon the phase, lattice plane and morphology. The X-Ray diffraction patterns of these CuS catalysts indicate the phases of these samples are similar, and can be indexed to the pattern of hexagonal phrase of CuS (as shown in Fig. 4-1), and crystallite size were 25.89-38.40 nm.. The scanning electron microscope images of prepared CuS samples are shown in Fig. 4-2. These particle sizes ranged from 250 to 500 nm. The light reflectance and bandgap energy strongly depends on the phase of the catalysts. Fig. 4-3 shows a series of UV-vis reflectance curves for the samples prepared by various CuS. All the samples exhibit similar reflectance curves. A significant increase in the reflectance at wavelengths about 564 ± 3.5 nm, and can be observed and the bandgap energy are estimated to be 1.88–2.04 eV according to the Tauc plot (as shown in Fig. 4-4).

4.1.1 **X-Ray Diffraction**

X-Ray diffraction was used to determine the phase and structure of the obtained products. The X-Ray diffraction patterns of 9 CuS samples synthesized with different mole ratios of copper-to-sulfur (1:6, 1:8 and 1:10) and synthesis times (24, 48 and 72 h) at 130℃ are presented in Fig. 4-1 and the cell parameters are a = 3.796 Å and c = 16.38 Å. The characteristic peaks of as-obtained CuS at 2θ = 27.9°, 29.4°, 32.4°, 46.4°and 54.8°can be perfectly corresponding to the (101), (102), (103), (110) and (108) in JCPDS card number 06-0464. All diffraction peaks were closely indexed with the standard peaks of CuS covellite (hexagonal) phase. Copper oxide or other impurity phases were not observed in the pattern, suggesting that the product was pure hexagonal copper sulfide (Saranya et al., 2014a). The intensity of (110) standard diffraction peak was particularly strong that may have some effects with the morphology of the products. Moreover, the results can confirm that 9 CuS samples were successfully synthesized with these conditions.

The average crystallite size of catalyst was estimated from the full width at half maximum (FWHM) of the most prominent X-Ray diffraction (110) broadening peak using Scherrer equation (Eq. 3-1). The results are shown in Table 4-1. For Cu:S = 1:6 with synthesis time 24, 48 and 72 h are corresponding to the crystallite size 33.39, 38.40 and 30.47 nm ; Cu:S = 1:8 with synthesis time 24, 48 and 72 h are corresponding to the crystallite size 33.54, 31.10 and 37.06 nm ; Cu:S = 1:10 with synthesis time 24, 48 and 72 h are corresponding to the crystallite size 32.08, 25.89 and 30.78 nm. The average is 32.52 ± 3.71 nm.

Table 4-1 Crystallite size analysis of as-prepared CuS.

Cu:S	Synthesis time (h)	(110) Peak intensity	FWHM (degree)	θ (degree)	Crystallite size (nm)
1:6	24	245	0.27046	23.19	33.39
	48	262	0.235105	23.16	38.40
	72	226	0.296418	23.19	30.47
1:8	24	250	0.269302	23.23	33.54
	48	201	0.290389	23.19	31.10
	72	252	0.243709	23.23	37.06
1:10	24	216	0.281477	23.19	32.08
	48	201	0.348963	23.27	25.89
	72	162	0.293378	23.19	30.78

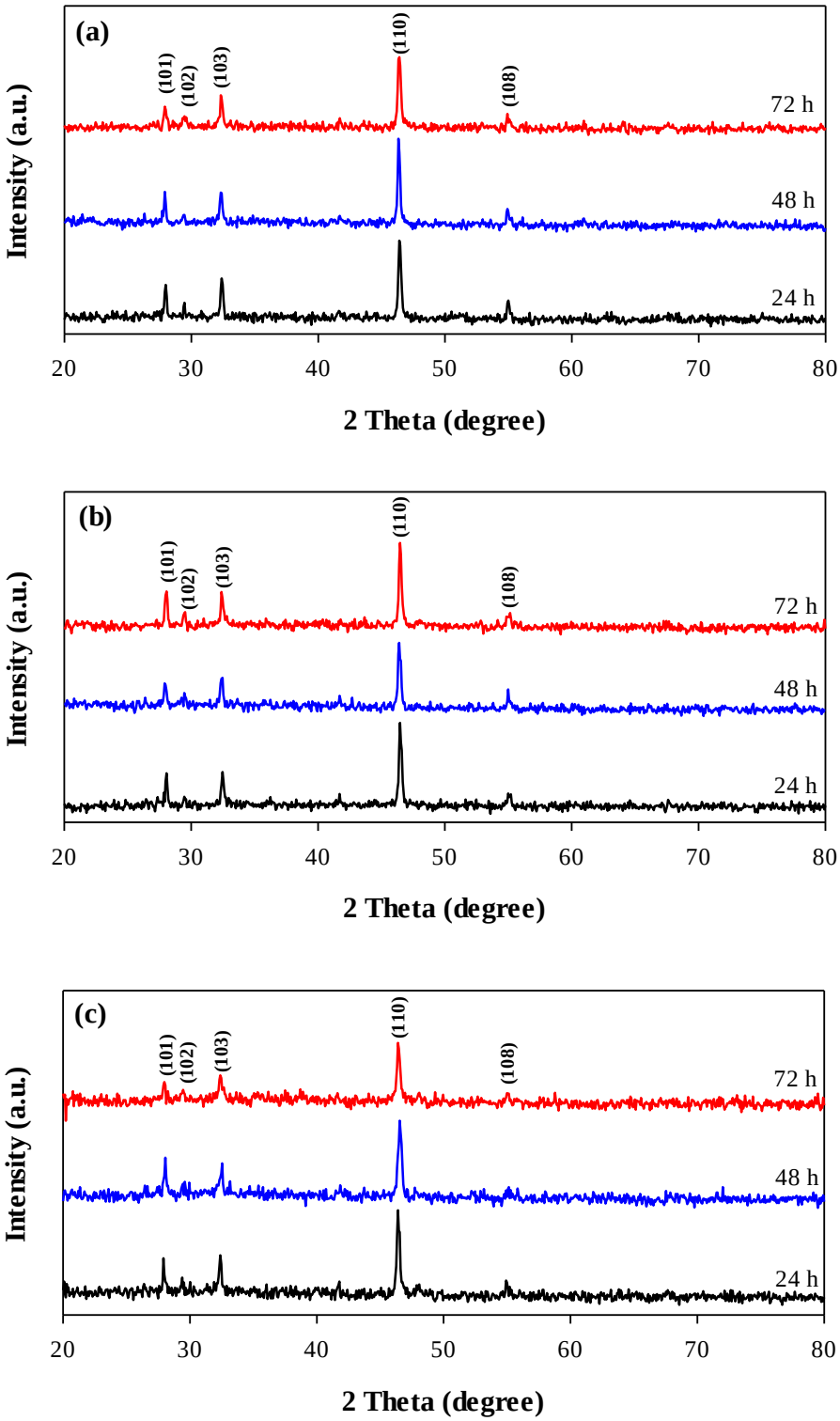

Fig. 4-1 XRD pattern of the prepared CuS obtained at 130℃

(a) Cu:S = 1:6 (b) Cu:S = 1:8 (c) Cu:S = 1:10

4.1.2 **Scanning Electron Microscope**

To know the effect of ratio of copper to sulfur and reaction time on the morphology of CuS, scanning electron microscope images of 9 samples are shown in Fig. 4-2. For copper-to-sulfur is 1:6 synthesis 24 h (Fig. 4-2a), the morphology presents an uneven particles distribution (size: 160–660 nm). For copper-to-sulfur is 1:6 synthesis 48 h (Fig. 4-2b), the morphology presents a uniform plates distribution (diameter: 200–330 nm, thickness: ~30 nm). For copper-to-sulfur is 1:6 synthesis 72 h (Fig. 4-2c), the morphology exhibits ~50% plates (diameter: 200–330 nm, thickness: ~30 nm) and ~50% hierarchical structures (size: 200–350 nm). For copper-to-sulfur is 1:8 synthesis 24 h (Fig. 4-2d), the morphology exhibits ~80% particles (size: 170–650 nm) and ~20% rope-like structures (length: 500–1100 nm, width: 160 nm). For copper-to-sulfur is 1:8 synthesis 48 h (Fig. 4-2e), the morphology exhibits ~50% particles (size: 130–330 nm), ~30% plates (diameter: 250–350 nm, thickness: ~30 nm) and ~20% hierarchical structures (size: 300–400 nm). For copper-to-sulfur is 1:8 synthesis 72 h (Fig. 4-2f), the morphology exhibits ~20% particles (size: 180–350 nm), ~50% plates (diameter: 250–350 nm, thickness: ~30 nm) and ~30% hierarchical structures (size: 300–400 nm). For copper-to-sulfur is 1:10 synthesis 24 h (Fig. 4-2g), the morphology exhibits ~50% particles (size: 300–500 nm) and ~50% rope-like structures (length: 500–1100 nm, width: 160 nm). For copper-to-sulfur is 1:10 synthesis 48 h (Fig. 4-2h), the morphology exhibits ~45% rope-like structures (length: 500–1100 nm, width: 160 nm), ~10% plates (diameter: 500–750 nm, thickness: ~30 nm) and ~45% hierarchical structures

(size: 300–400 nm). For copper-to-sulfur is 1:10 synthesis 72 h (Fig. 4-2i), the morphology presents a uniform plate-like hierarchical structures distribution (diameter: 300–500 nm, thickness: ~30 nm).

Therefore, the morphology of CuS becomes rope-like structure from particle with the increasing of the proportion of sulfur doped and becomes hierarchical structure when increasing of synthesis times. The more complex structures (plate, rope-like and hierarchical structure) are obtained with increased sulfur content and reaction times.

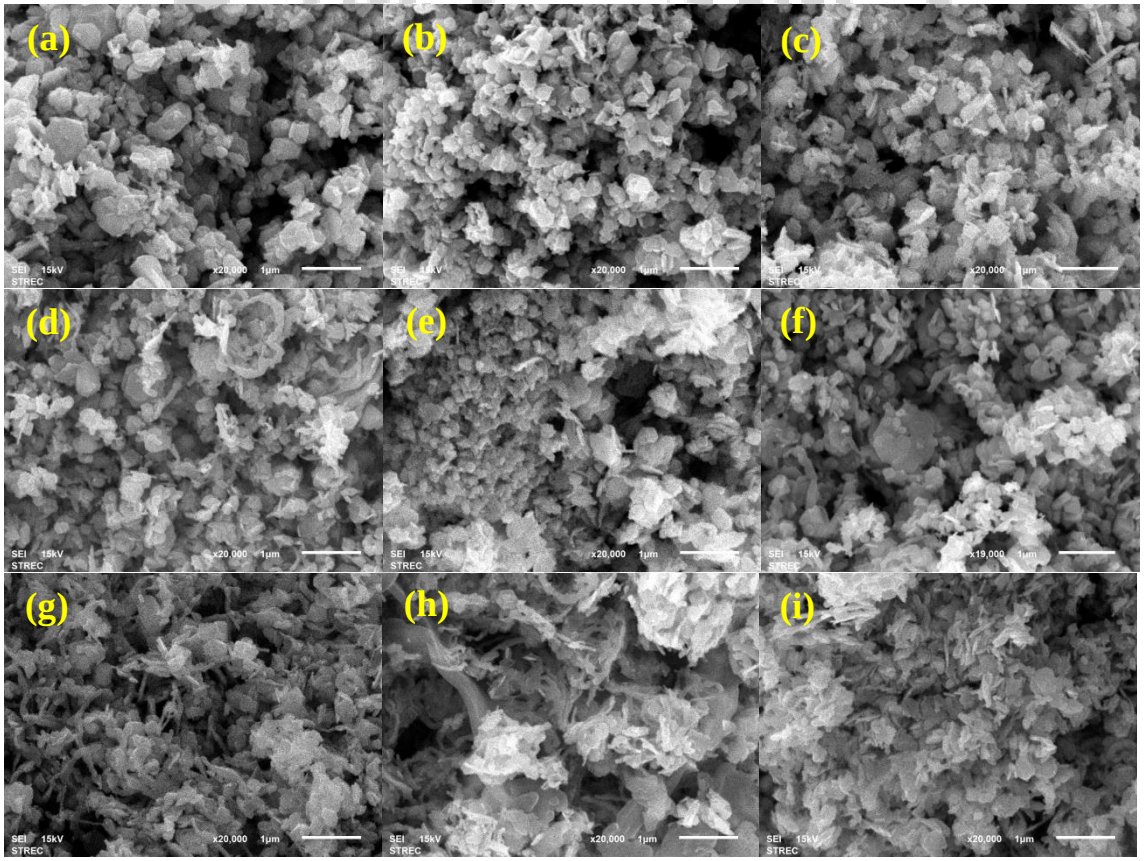

Fig. 4-2 SEM images of the prepared CuS obtained at 130℃.
(a) Cu:S = 1:6 obtained for 24 h (b) Cu:S = 1:6 obtained for 48 h
(c) Cu:S = 1:6 obtained for 72 h (d) Cu:S = 1:8 obtained for 24 h
(e) Cu:S = 1:8 obtained for 48 h (f) Cu:S = 1:8 obtained for 72 h
(g) Cu:S = 1:10 obtained for 24 h (h) Cu:S = 1:10 obtained for 48 h
(i) ratio Cu:S 1:10 obtained for 72 h

4.1.3 **UV-Vis Diffuse Reflectance Spectroscopy**

UV-Vis Diffuse Reflectance spectra of all CuS samples are shown in Fig. 4-3. The characteristic peak of various CuS is at 564 ± 3.5 nm.

The Tauc plot (Tauc, 1968; Pop et al., 2011) prepared to estimate the energy band-gap of all CuS samples. They were plotted of the Tauc plot $(\alpha h\nu)^2$ that converted from spectra versus photon energy ($h\nu$), where α is the absorption coefficient, h is the Planck constant, ν is the light frequency, as shown in Fig. 4-4. The linear extrapolation was a tangent line drawn through the maximum slope and taken the intersection with the x-axis. As a result shown in Table 4-2, energy band-gap of the prepared CuS obtained at 130℃ with various sulfur content and synthesis times are between 1.88 and 2.04 eV, the average is 1.96 ± 0.048 eV. The energy band-gap of as-prepared CuS all correspond in range of reference review on Table 2-1 and Table 2-2 (E_g =1.27 - 3.38 eV).

Table 4-2 Energy band-gap of the prepared CuS obtained at 130℃

	Synthesis time	Cu:S 1:6	Cu:S 1:8	Cu:S 1:10
E_g (eV)	24 h	1.91	2.04	1.94
	48 h	1.88	1.93	1.98
	72 h	1.98	1.98	1.99

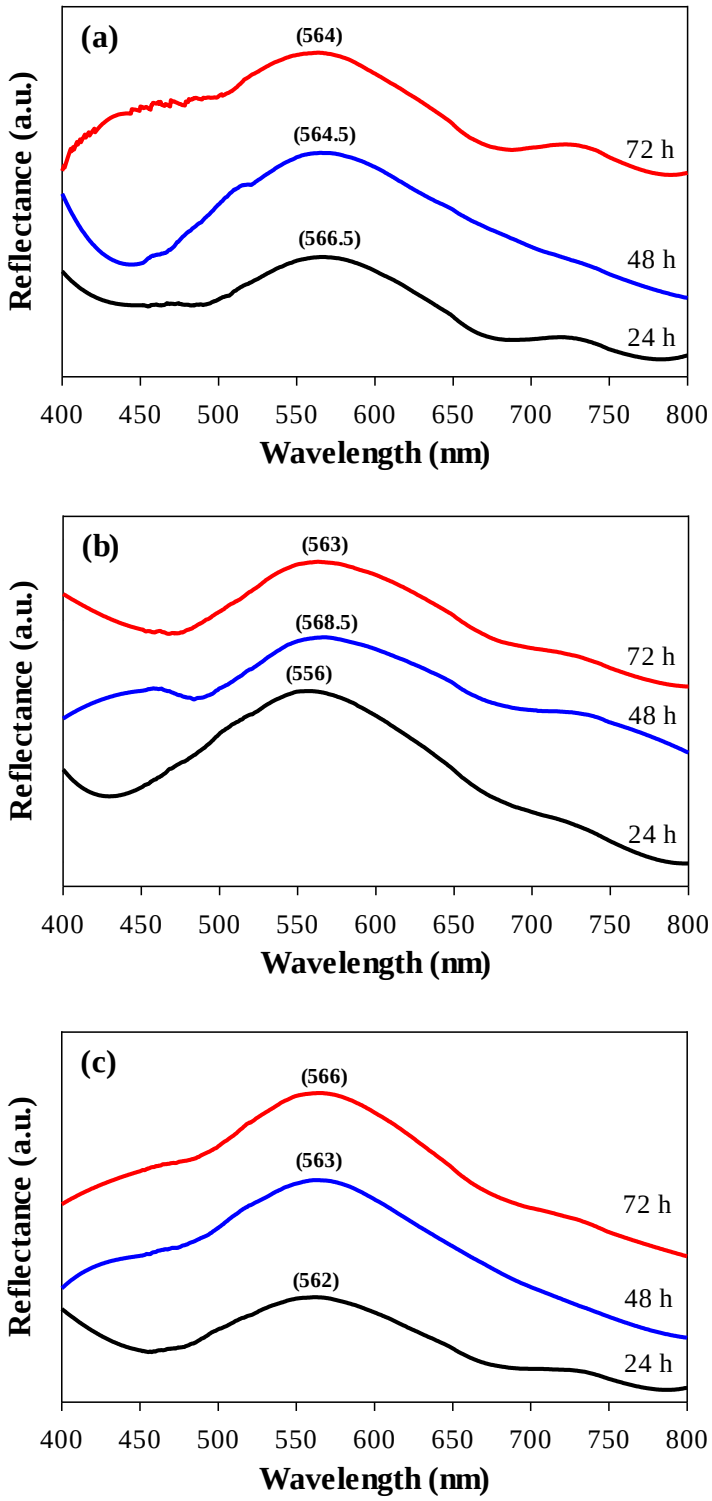

Fig. 4-3 UV-Vis DRS spectra of the prepared CuS obtained at 130℃

(a) Cu:S = 1:6 (b) Cu:S = 1:8 (c) Cu:S = 1:10

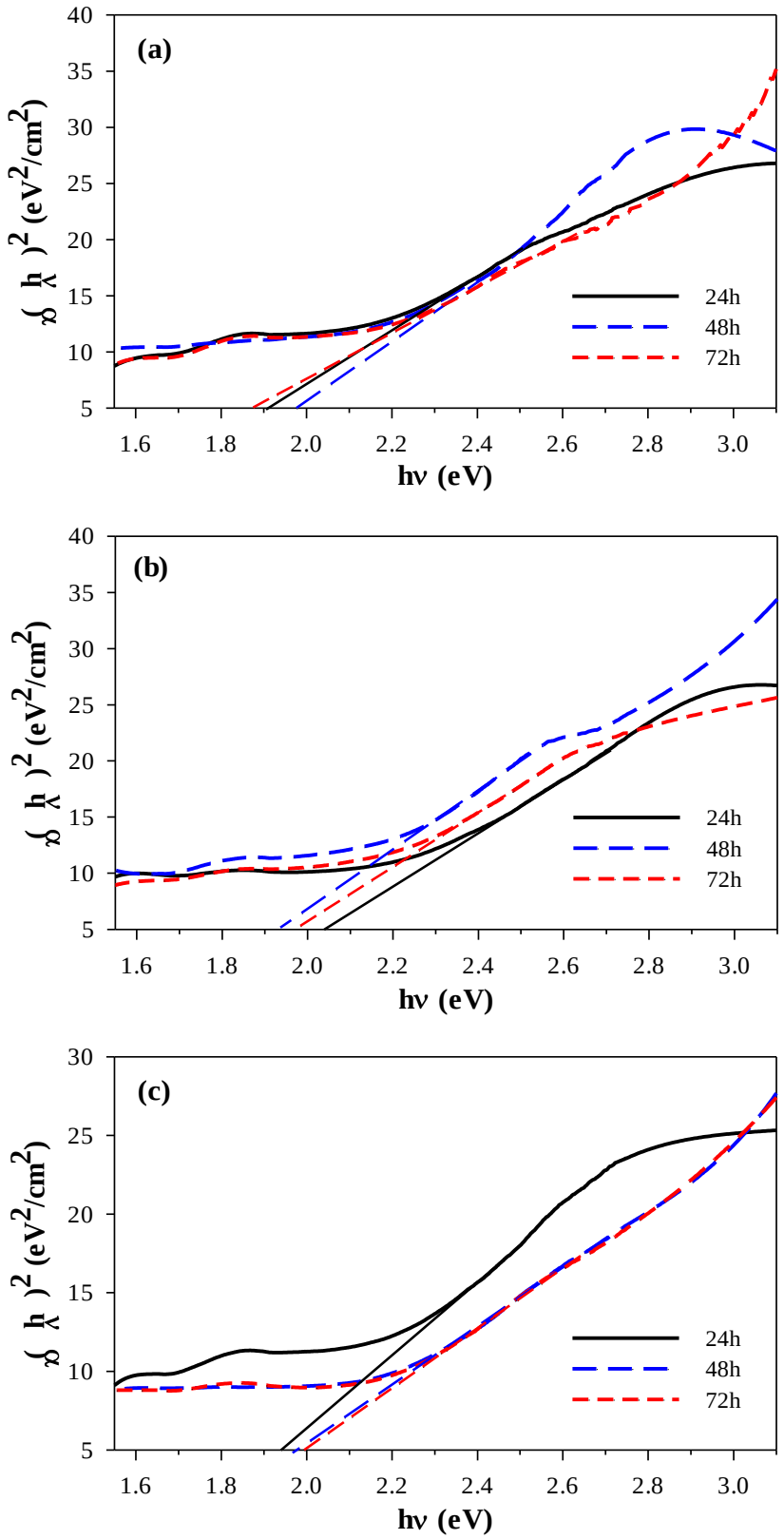

Fig. 4-4 Band-gap spectra of the prepared CuS obtained at 130℃

(a) Cu:S = 1:6 (b) Cu:S = 1:8 (c) Cu:S = 1:10

4.1.4 **Effect of Copper-to-Sulfur Molar Ratios and Synthesis Time**

From the SEM images of the prepared CuS (Fig. 4-2) and Table 4-3 to study morphology of CuS, it becomes rope-like structure from particle with the increasing of the proportion of sulfur doped and becomes hierarchical structure when increasing of synthesis times. The more complex structures (plate, rope-like and hierarchical structure) are obtained with increased sulfur content and reaction times.

Sulfur plays an important role not only in precipitating the particles but also in controlling the size and stability of the particles (Dixit et al., 1998). However, changing the copper-to-sulfur molar ratio did not affect the crystallinity of the obtained products, indeed line broadening analysis on the (110) reflection at 23.2° via the Scherrer equation (Eq. 3-1) reveals the crystallite size remains 32.52 ± 3.71 nm across the series. SEM reveals however that the morphology of agglomerated CuS crystals does evolve as a function of the Cu:S molar ratio. At high Cu:S ratios (Cu-rich) $Na_2S \cdot 9H_2O$ acts only as the sulfur precursor forming CuS particle with non-uniform size. The fact crystallite size from XRD is invariant of Cu:S ratio suggests these particles are agglomerates of crystals. (Thuy et al., 2014)

Table 4-3 Effect of sulfur content and synthesis time for morphology of CuS

Cu:S	Synthesis time (h)	Crystallite size (nm)	E_g (eV)	Morphology
1: 6	24	33.39	1.91	particles (size: 160–660 nm)
	48	38.4	1.88	plates (diameter: 200–330 nm, thickness: ~30 nm)
	72	30.47	1.98	~50% plates (diameter: 200–330 nm, thickness: ~30 nm), ~50% hierarchical structures (size: 200–350 nm)
1: 8	24	33.54	2.04	~80% particles (size: 170–650 nm), ~20% rope-like structures (length: 500–1100 nm, width: 160 nm)
	48	31.1	1.93	~50% particles (size: 130–330 nm), ~30% plates (diameter: 250–350 nm, thickness: ~30 nm), ~20% hierarchical structures (size: 300–400 nm)
	72	37.06	1.98	~20% particles (size: 180–350 nm), ~50% plates (diameter: 250–350 nm, thickness: ~30 nm), ~30% hierarchical structures (size: 300–400 nm)
1: 10	24	32.08	1.94	~50% particles (size: 300–500 nm), ~50% rope-like structures (length: 500–1100 nm, width: 160 nm)
	48	25.89	1.98	~45% rope-like structures (length: 500–1100 nm, width: 160 nm), ~10% plates (diameter: 500–750 nm, thickness: ~30 nm), ~45% hierarchical structures (size: 300–400 nm)
	72	30.78	1.99	plate-like hierarchical structures (diameter: 300–500 nm, thickness: ~30 nm)

4.2 Fenton-like Photocatalytic Degradation of Paraquat

The photocatalytic activities of CuS were studied by the degradation of paraquat solution with catalyst dosage 1.0 g/L and hydrogen peroxide dosage 0.22 M under visible light while irradiance equal to 6 W/m^2, and the measurement was taken using a UV-vis spectrophotometer with a detector set at λ = 257 nm. An analysis of all studied catalysts on the paraquat degradation was carried out in the dark for 60 min before the photocatalysis study to reach the equilibrium.

4.2.1 Comparison between CuS and TiO_2

The results of degraded paraquat solution (40 mg/L) that tested by CuS (Cu:S = 1:10, synthesis 72h) and TiO_2 P25 with catalyst dosage 1.0 g/L. The effect of hydrogen peroxide (H_2O_2) addition is shown in Fig. 4-5. The CuS with H_2O_2 could be degraded by 100%, less than 20% on TiO_2 with H_2O_2 and less than 7% with only H_2O_2. The presence of H_2O_2 can enhance the photodegradation of paraquat due to H_2O_2 is an electron acceptor that can overcome the drawback of charge recombination (Kitsiou et al., 2009). For TiO_2 with H_2O_2 case, it just removed few contaminant by surface adsorption instead of photocatalysis, owing to the absorption of photon energy ($h\nu$) from visible light illumination was not higher than or equal to energy band-gap of TiO_2 (3.2 eV) (Wang et al., 2014a).

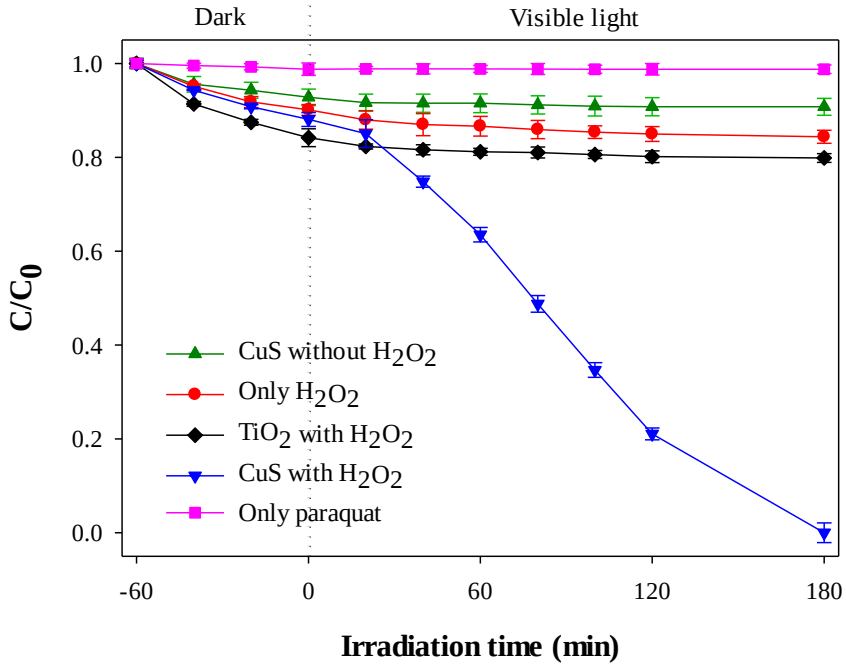

Fig. 4-5 Photocatalytic degradations of 40 mg/L paraquat under 6 W/m^2 visible light irradiation using CuS (Cu:S = 1:10, 72h) and TiO_2 P25 with catalyst dosage 1.0 g/L, and H_2O_2 dosage 0.22 M.

4.2.2 Mechanism of Fenton-like Photocatalytic Degradation

To explore the degeneration mechanism of CuS as photocatalyst combine with photo-Fenton-like oxidation, similar degeneration experiments were preceded in different conditions. As shown in Fig. 4-5, the paraquat was degenerated barely without CuS and H_2O_2, which indicates that paraquat is stable in the solution. The concentration of paraquat solution does not decrease less than 1% that tested by Copper sulfide (CuS) without H_2O_2 because the energy positions of conduction and valance band of CuS were lower than water stability line (Xu and Schoonen, 2000). So the Cu^+ in the CuS could react with H_2O_2 to generate hydroxyl radicals, and further improve the photocatalytic property. On

the other hand, photogenerated electron on the CuS can transfer from the valence band to the conduction band, and accordingly, a photogenerated hole can be formed. The photogenerated hydroxyl radicals can be produced by the reaction between the photogenerated hole and H_2O. H_2O_2 is an efficient electron acceptor, the H_2O_2 can promote the separation of the photogenerated electron and hole, and more photogenerated hydroxyl radicals can be generated in the presence of H_2O_2 (Xu et al., 2015). The paraquat solution can react with the hydroxyl radicals both generated from Fenton-like reactions and photocatalysis.

The paraquat degradation in H_2O_2 solution can be explained by the photo-Fenton reactions, i.e. the hemolytic cleavage of H_2O_2:

$$H_2O_2 \rightarrow 2HO^{\bullet} \qquad \text{(Eq. 4-2)}$$

In aqueous solution, the effect of water molecules would decrease the primary quantum caused by combination of hydroxyl radicals:

$$2(H_2O_2 + HO^{\bullet}) \rightarrow H_2O + HO_2^{\bullet} \qquad \text{(Eq. 4-3)}$$

$$2HO_2^{\bullet} \rightarrow H_2O_2 + O_2 \qquad \text{(Eq. 4-4)}$$

The CuS exhibits catalytic activity with the help of H_2O_2. This makes it possible that Cu^+ in the CuS reacts with H_2O_2 generates hydroxyl radicals, and further leads to a Fenton-like reaction which can be deduced as follows (Li et al., 2012):

$$H_2O_2 + Cu^+ \rightarrow Cu^{2+} + OH^- + HO^{\bullet} \qquad \text{(Eq. 4-5)}$$

$$Cu^{2+} + H_2O_2 \rightarrow Cu^{+} + HO_2^{\bullet} + H^{+} \qquad \text{(Eq. 4-6)}$$

Therefore, $OH^{\bullet}$ radicals can attack paraquat as below:

$$RH + HO^{\bullet} \rightarrow CO_2 + H_2O \qquad \text{(Eq. 4-7)}$$

The mechanism of Fenton-like photocatalytic degradation of paraquat using CuS catalysts can be illustrated on Fig. 4-6. There has two ways to decompose paraquat. One is direct decomposition via redox reactions from electron-hole pairs on the CuS surface. Another one is indirect decomposition by hydroxyl radicals ($OH^{\bullet}$) in surroundings solution. And the presence of H_2O_2 generated more $HO^{\bullet}$ from 2 pathways (photogenerated by hv and reduction of e^{-}) made contributions to the oxidation of the paraquat molecules.

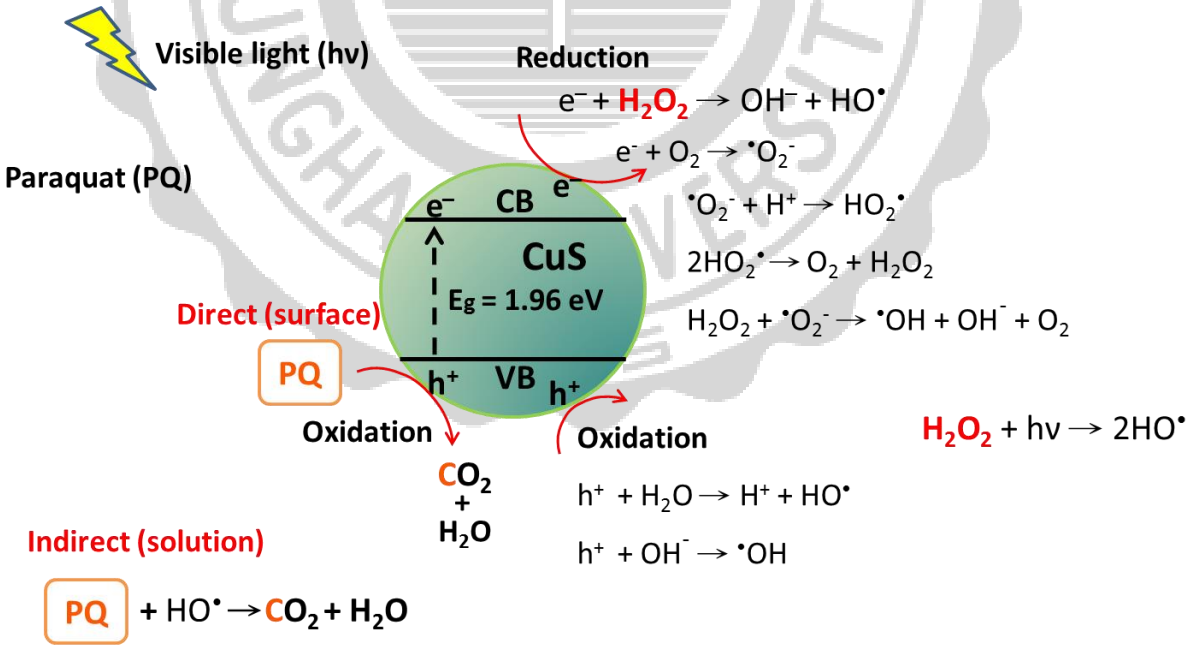

Fig. 4-6 The mechanism of Fenton-like photocatalytic degradation of paraquat using CuS catalysts

4.3 Kinetic Study of Photocatalysis

4.3.1 Comparison between Various CuS

Fig. 4-7 shows the photocatalytic degradations of 40 mg/L paraquat solution using 9 CuS samples with catalyst dosage 1.0 g/L, and hydrogen peroxide dosage 0.22 M under visible light while irradiance equal to 6 W/m^2. An analysis of all studied catalysts on the paraquat degradation was carried out in the dark for 60 min before the photocatalysis study to reach the equilibrium.

In addition, 40 mg/L paraquat can be 100% degraded within 240 min for 9 CuS samples. The kinetics of reaction was expressed by pseudo-first order (Eq. 3-3) in Langmuir-Hinshelwood kinetic model. The results of observed rate constant (k_{obs}) and initial rate (r_0) for 9 as-prepared CuS illustrate on

Table 4-4. CuS which has better photocatalytic performance was Cu:S = 1:8 via hydrothermal treatment for 72 h with observed rate constant $k_{obs} = 2.0\times10^{-2}$ (1/min) and initial rate $r_0 = 0.251\times10^{-2}$ (mM/min).

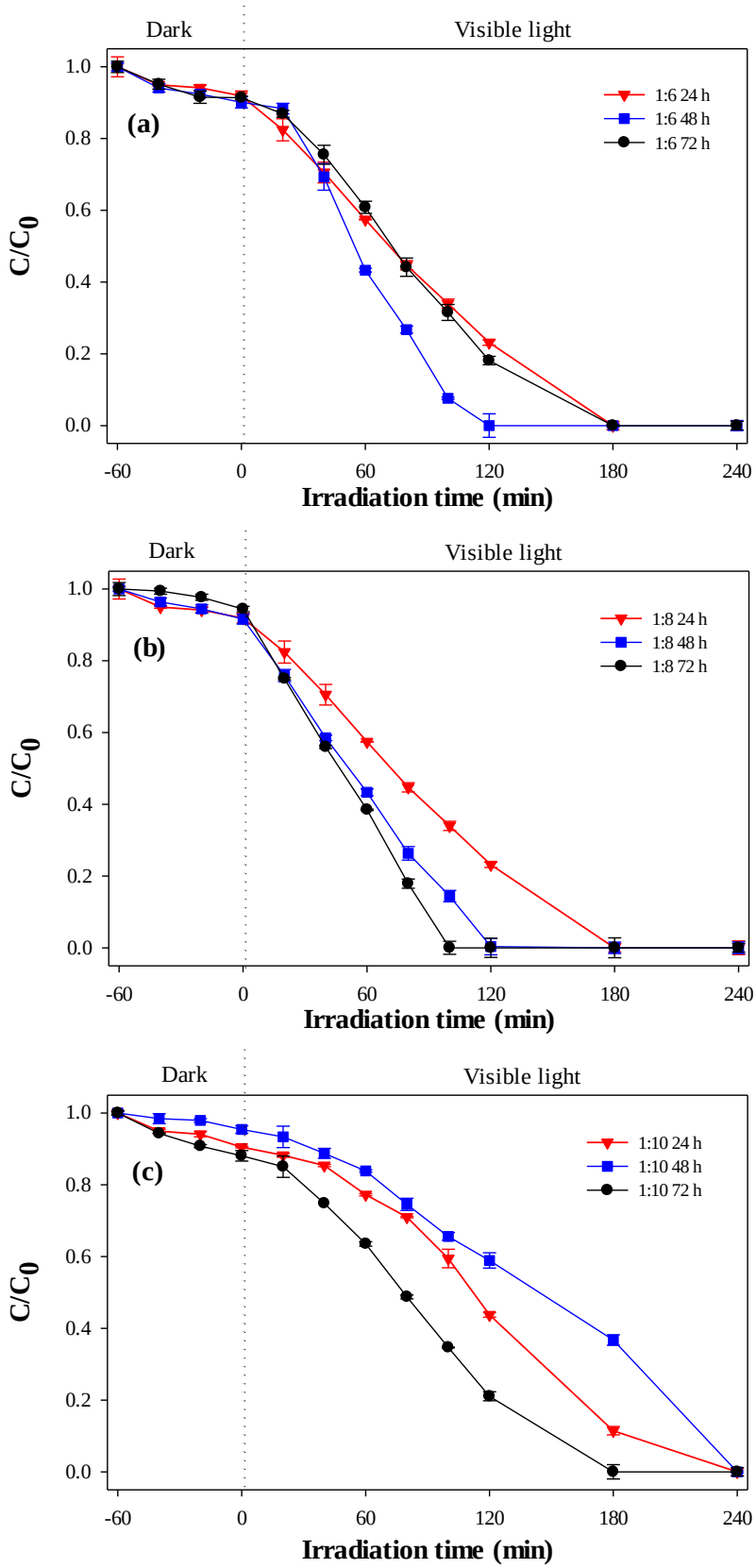

Fig. 4-7 Photocatalytic degradations of 40 mg/L paraquat solution in presence of 0.22 M H_2O_2 under 6 W/m^2 visible light irradiation using 9 CuS with dosage 1.0 g/L.

Table 4-4 Kinetic evolution of paraquat photodegradation for various CuS.

Cu:S	Synthesis time (h)	Crystallite size (nm)	E_g (eV)	C_0 (mM)	$k_{obs}\times10^{-2}$ (1/min)	$r_0\times10^{-2}$ (mM/min)
1:6	24	33.39	1.91	0.143173	0.901	0.1290
	48	38.4	1.88	0.123723	1.570	0.1942
	72	30.47	1.98	0.142676	0.906	0.1293
1:8	24	33.54	2.04	0.146823	0.933	0.1370
	48	31.1	1.93	0.127169	1.530	0.1946
	72	37.06	1.98	0.12571	2.000	0.2514
1:10	24	32.08	1.94	0.13006	0.309	0.0402
	48	25.89	1.98	0.158563	0.320	0.0507
	72	30.78	1.99	0.129184	0.737	0.0952

4.3.2 **Effect of Initial Paraquat Concentrations**

In Table 4-4, we chose one of 9 as-prepared CuS which has the second better photocatalytic performance (Cu:S = 1:6, 48 h with k_{obs} = 1.57×10^{-2} (1/min) and r_0 = 0.1942×10^{-2} (mM/min), lower cost and friendly to environment. To study photocatalysis kinetic of CuS were evaluated by degradation efficiency of different concentration paraquat (20, 40, 60, 80, 100 mg/L) using CuS that Cu:S = 1:6 synthesized 48 h.

The Langmuir-Hinshelwood adsorption equilibrium constant and the surface reaction rate constant can be estimate from the slope and intercept of Eq. 3-7 that plotted of $1/r_0$ versus $1/C_0$ in Fig. 4-8. Ultimately, the Langmuir-Hinshelwood adsorption equilibrium constant (K_a) and the surface reaction rate constant (k_r)

of paraquat degradation were 10.34/mM and 2.5×10^{-3}/min, respectively. It confirmed that the CuS can reveal photocatalytic activity of paraquat solution and follow the as-estimated equation (Eq. 4-1).

$$\frac{1}{r_0} = \frac{38.259}{C_0} + 395.747 \qquad \text{(Eq. 4-1)}$$

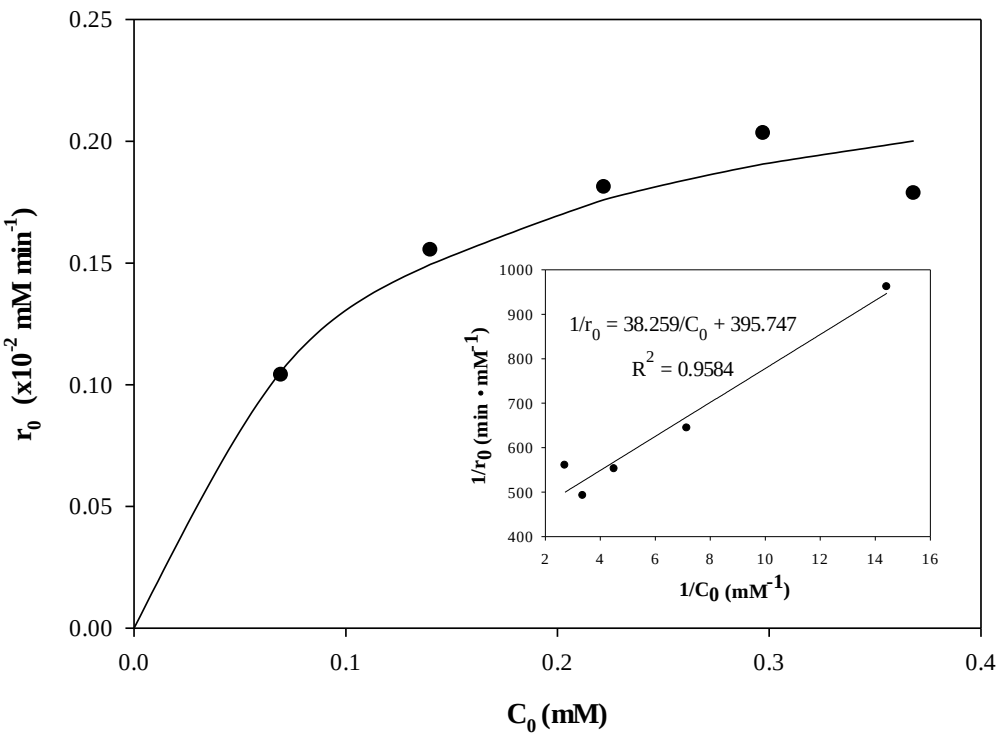

Fig. 4-8 Plot of initial rate method for kinetic evaluations.

Chapter 5 Conclusions and Recommendations

5.1 Conclusions

(1) CuS photocatalysts were successfully prepared by hydrothermal method from the solution of $CuCl_2 \cdot 2H_2O$ and $Na_2S \cdot 9H_2O$ by employing CTAB as a reducing agent at 130℃. CuS exists hexagonal phase and crystallite size were 25.89-38.40 nm. The particles size ranged from 250 to 500 nm. Energy band-gap was in range of 1.88–2.04 eV. The more complex structures (plate, rope-like and hierarchical structure) are obtained with increased sulfur content and reaction times.

(2) CuS has better photocatalytic performances then the commercial TiO_2 P25 for degrading 40 mg/L paraquat under visible light in the presence of H_2O_2. And the presence of H_2O_2 generated more $HO^{\bullet}$ from two pathways (photogenerated by hν and reduction of e^-) made contributions to the oxidation of the paraquat molecules. Paraquat was oxidized by h^+ on the CuS surface (direct decomposition) and $HO^{\bullet}$ in the solution (indirect decomposition).

(3) CuS achieved an optimal photocatalytic performance when Cu:S = 1:8 for 72 h, followed pseudo-first order with an observed rate constant (k_{obs}) of 2.0×10^{-2} /min and initial reaction rate (r_0) of 0.251×10^{-2} mM/min.

(4) The paraquat photocatalytic degradation kinetic model fit well with Langmuir–Hinshelwood rate law. The Langmuir-Hinshelwood adsorption

equilibrium constant (Ka) = 10.34 /mM, and the surface reaction rate constant (kr) = 2.5×10^{-3} /min.

5.2 Recommendations

(1) To probe the atomic composition of elements present in the as-prepared CuS by X-ray fluorescence spectroscopy (XRF) or energy dispersive X-ray spectrometry (EDS).

(2) Formation reaction of CuS ($CuCl_2$ + Na_2S) should be discussed.

(3) The effect of various dosages of H_2O_2 and CuS in heterogeneous photo-Fenton-like oxidation system should be investigated. To establish an optimal parameter for degrading system.

(4) Mechanism pathway (intermediates) of paraquat photocatalytic degradation over CuS with H_2O_2 under visible irradiation should be characterized by HPLC or GC/MS.

(5) Recyclability of CuS should be given consideration to characterize the photocatalytic performance.

REFERENCE

An, J., Zhu, L., Zhang, Y., and Tang, H. (2013). Efficient visible light photo-Fenton-like degradation of organic pollutants using in situ surface-modified $BiFeO_3$ as a catalyst. *Journal of Environmental Sciences, 25*(6), 1213-1225.

Andreozzi, R., Insola, A., Caprio, V., and D'Amore, M. G. (1993). Ozonation of 1, 1' dimethyl, 4,4' bipyridinium dichloride (Paraquat) in aqueous solution. *Environmental Technology, 14*(7), 695-700.

Awodugba, A. O., and Ibiyemi, A. A. (2012). Optical Properties and Band Offsets of CuS/ZnS Supperlattice. *The Pacific Journal of Science and Technology, 13*, 206-212.

Bismuth, C., Scherrmann, J. M., Garnier, R., Baud, F. J., and Pontal, P. G. (1987). Elimination of paraquat. *Human and Experimental Toxicology, 6*(1), 63-67.

Bromilow, R. H. (2004). Paraquat and sustainable agriculture. *Pest Management Science, 60*(4), 340-349.

Cantavenera, M. J., Catanzaro, I., Loddo, V., Palmisano, L., and Sciandrello, G. (2007). Photocatalytic degradation of paraquat and genotoxicity of its intermediate products. *Journal of Photochemistry and Photobiology A: Chemistry, 185*, 277-282.

Cartaxo, M. A. M., Borges, C. M., Pereira, M. I. S., and Mendonça, M. H. (2015). Electrochemical oxidation of paraquat in neutral medium. *Electrochimica Acta, 176*, 1010-1018.

Chen, C., Cai, W., Long, M., Zhou, B., Wu, Y., Wu, D., and Feng, Y. (2010). Synthesis of Visible-Light Responsive Graphene Oxide/TiO2 Composites with p/n Heterojunction. *ACS Nano, 4*(11), 6425-6432.

Darouie, M., Afshar, S., Zare, K., and Monajjemi, M. (2013). Investigation of different factors towards synthesis of CuS spherical nanoparticles. *Journal of Experimental Nanoscience, 8*(4), 451-461.

Deng, C., Ge, X., Hu, H., Yao, L., Han, C., and Zhao, D. (2014). Template-free and green sonochemical synthesis of hierarchically structured CuS hollow microspheres displaying excellent Fenton-like catalytic activities. *CrystEngComm, 16*(13), 2738-2745.

Dhaouadi, A., and Adhoum, N. (2010). Heterogeneous catalytic wet peroxide oxidation of paraquat in the presence of modified activated carbon. *Applied Catalysis B: Environmental, 97*(1-2), 227-235.

Dixit, S. G., Mahadeshwar, A. R., and Haram, S. K. (1998). Some aspects of the role of surfactants in the formation of nanoparticles. *Colloids and Surfaces A: Physicochemical and Engineering Aspects, 133*(1), 69-75.

Fenton, H. J. H. (1894). LXXIII.-Oxidation of tartaric acid in presence of iron. *Journal of the Chemical Society, Transactions, 65*(0), 899-910.

Fujishima, A., and Honda, K. (1972). Electrochemical Photolysis of Water at a Semiconductor Electrode. *Nature, 238*(5358), 37-38.

Glaze, W. H., Kang, J.-W., and Chapin, D. H. (1987). The Chemistry of Water Treatment Processes Involving Ozone, Hydrogen Peroxide and Ultraviolet Radiation. *Ozone: Science and Engineering, 9*(4), 335-352.

Gordon, I., Conibeer, G., Krc, J., Slaoui, A., Niki, S., Ghribi, F., Alyamani, A., Ayadi, Z. B., Djessas, K., and Mir, L. E. (2015). Proceedings of the EMRS 2015 Spring meeting – Symposium C on Advanced Inorganic Materials and Structures for

PhotovoltaicsStudy of CuS Thin Films for Solar Cell Applications Sputtered from Nanoparticles Synthesised by Hydrothermal Route. *Energy Procedia, 84*, 197-203.

Gupta, V. K., Pathania, D., Agarwal, S., and Singh, P. (2012). Adsorptional photocatalytic degradation of methylene blue onto pectin-CuS nanocomposite under solar light. *Journal of Hazardous Materials, 243*, 179-186.

Gurin, V. S., Prakapenka, V. B., Kovalenko, D. L., and Alexeenko, A. A. (2003). Sol-Gel Derived Silica Films with Ultrafine Copper, Copper Sulfide and Copper Selenide Particles. *Journal of Sol-Gel Science and Technology, 26*(1), 961-966.

Hamadi, N. K., Sri, S., and Chen, X. D. (2004). Adsorption of Paraquat dichloride from aqueous solution by activated carbon derived from used tires. *Journal of Hazardous Materials, 112*(1-2), 133-141.

Hu, X.-S., Shen, Y., Xu, L.-H., Wang, L.-M., Lu, L.-s., and Zhang, Y.-t. (2016). Preparation of flower-like CuS by solvothermal method for photocatalytic, UV protection and EMI shielding applications. *Applied Surface Science, 385*, 162-170.

Kitsiou, V., Filippidis, N., Mantzavinos, D., and Poulios, I. (2009). Heterogeneous and homogeneous photocatalytic degradation of the insecticide imidacloprid in aqueous solutions. *Applied Catalysis B: Environmental, 86*(1-2), 27-35.

Kundu, J., and Pradhan, D. (2014). Controlled synthesis and catalytic activity of copper sulfide nanostructured assemblies with different morphologies. *ACS Applied Materials and Interfaces, 6*(3), 1823-1834.

Lee, S. J., Katayama, A., and Kimura, M. (1995). Microbial degradation of paraquat sorbed to plant residues. *Journal of Agricultural and Food Chemistry, 43*(5), 1343-1347.

Li, F., Wu, J., Qin, Q., Li, Z., and Huang, X. (2010). Controllable synthesis, optical and photocatalytic properties of CuS nanomaterials with hierarchical structures. *Powder Technology, 198*(2), 267-274.

Li, S., Ge, Z.-H., Zhang, B.-P., Yao, Y., Wang, H.-C., Yang, J., Li, Y., Gao, C., and Lin, Y.-H. (2016). Mechanochemically synthesized sub-5nm sized CuS quantum dots with high visible-light-driven photocatalytic activity. *Applied Surface Science, 384*, 272-278.

Li, Z., Mi, L., Chen, W., Hou, H., Liu, C., Wang, H., Zheng, Z., and Shen, C. (2012). Three-dimensional CuS hierarchical architectures as recyclable catalysts for dye decolorization. *CrystEngComm, 14*(11), 3965.

Mechakra, H., Sehili, T., Kribeche, M. A., Ayachi, A. A., Rossignol, S., and George, C. (2016). Use of natural iron oxide as heterogeneous catalyst in photo-Fenton-like oxidation of chlorophenylurea herbicide in aqueous solution: Reaction monitoring and degradation pathways. *Journal of Photochemistry and Photobiology A: Chemistry, 317*, 140-150.

Mi, L., Wei, W., Zheng, Z., Gao, Y., Liu, Y., Chen, W., and Guan, X. (2013). Tunable properties induced by ion exchange in multilayer intertwined CuS microflowers with hierarchal structures. *Nanoscale, 5*(14), 6589-6598.

Miguel, N., Ormad, M. P., Mosteo, R., and Ovelleiro, J. L. (2012). Photocatalytic Degradation of Pesticides in Natural Water: Effect of Hydrogen Peroxide. *International Journal of Photoenergy, 2012*, 1-11.

Mills, A., O'Rourke, C., and Moore, K. (2015). Powder semiconductor photocatalysis in aqueous solution: An overview of kinetics-based reaction mechanisms. *Journal of Photochemistry and Photobiology A: Chemistry, 310*, 66-105.

Moctezuma, E., Leyva, E., Monreal, E., Villegas, N., and Infante, D. (1999). Photocatalytic degradation of the herbicide “Paraquat”. *Chemosphere, 39*(3), 511-517.

Mousavi-Kamazani, M., Salavati-Niasari, M., and Ramezani, M. (2013). Preparation and Characterization of Cu2S Nanoparticles Via Ultrasonic Method. *Journal of Cluster Science, 24*(3), 927-934.

Naşcu, C., Pop, I., Ionescu, V., Indrea, E., and Bratu, I. (1997). Spray pyrolysis deposition of CuS thin films. *Materials Letters, 32*(2), 73-77.

Nezamzadeh-Ejhieh, A., and Moazzeni, N. (2013). Sunlight photodecolorization of a mixture of Methyl Orange and Bromocresol Green by CuS incorporated in a clinoptilolite zeolite as a heterogeneous catalyst. *Journal of Industrial and Engineering Chemistry, 19*(5), 1433-1442.

Nimtz, G. (1980). Recombination in narrow-gap semiconductors. *Physics Reports, 63*(5), 265-300.

Pop, A. E., Popescu, V., Danila, M., and Batin, M. N. (2011). Optical properties of CuxS nano-powders. *Chalcogenide Letters, 8*(6), 363-370.

Rajendran, V., and Gajendiran, J. (2015). Nonionic surfactant poly (ethane 1,2-diol)-400 assisted solvothermal synthesis of copper monosulfide (CuS) nanoplates and their structural, topographical, optical and luminescent properties. *Materials Science in Semiconductor Processing, 36*, 92-95.

Santos, M. S. F., Alves, A., and Madeira, L. M. (2011). Paraquat removal from water by oxidation with Fenton's reagent. *Chemical Engineering Journal, 175*, 279-290.

Saranya, M., Ramachandran, R., Samuel, E. J. J., Jeong, S. K., and Grace, A. N. (2015). Enhanced visible light photocatalytic reduction of organic pollutant and electrochemical properties of CuS catalyst. *Powder Technology, 279*, 209-220.

Saranya, M., Santhosh, C., Ramachandran, R., Kollu, P., Saravanan, P., Vinoba, M., Jeong, S. K., and Grace, A. N. (2014a). Hydrothermal growth of CuS nanostructures and its photocatalytic properties. *Powder Technology, 252*, 25-32.

Saranya, M., Santhosh, C., Ramachandran, R., and Nirmala Grace, A. (2014b). Growth of CuS Nanostructures by Hydrothermal Route and Its Optical Properties. *Journal of Nanotechnology, 2014*, 8.

Shamraiz, U., Hussain, R. A., and Badshah, A. (2016). Fabrication and applications of copper sulfide (CuS) nanostructures. *Journal of Solid State Chemistry, 238*, 25-40.

Simonescu, C. M., Teodorescu, V. S., and Capatina, C. (2008). Surfactant involved in Copper Sulfide Nanocrystallites Synthesis. *Revista De Chimie, 59*(12), 1327-1329.

Singh, B., and Singh, K. (2016). Microbial degradation of herbicides. *Critical Reviews in Microbiology, 42*(2), 245-261.

Slade, P., and Calderblank, A. (1975). In Herbicides: Chemistry, Degradation and Mode of Action. In K. P. C. and K. D. .D. (Eds.), (2 nd ed.). New York: M. Dekker.

Sohrabnezhad, S., Zanjanchi, M. A., Hosseingholizadeh, S., and Rahnama, R. (2014). Facile and low temperature route to synthesis of CuS nanostructure in mesoporous material by solvothermal method. *Spectrochimica Acta Part A: Molecular and Biomolecular Spectroscopy, 123*, 142-150.

Somich, C. J., Muldoon, M. T., and Kearney, P. C. (1990). On-site treatment of pesticide waste and rinsate using ozone and biologically active soil. *Environmental Science and Technology, 24*(5), 745-749.

Suja, R., Geetha, D., and Ramesh, P. (2013). Preparation and characterization of CuS

Nanomaterials by solvothermal method. *International Journal of Scientific and Engineering Research, 4*(3).

Suri, R. P. S., Liu, J., Hand, D. W., Crittenden, J. C., Perram, D. L., and Mullins, M. E. (1993). Heterogeneous Photocatalytic Oxidation of Hazardous Organic Contaminants in Water. *Water Environment Research, 65*(5), 665-673.

Tanveer, M., Cao, C., Aslam, I., Ali, Z., Idrees, F., Tahir, M., Khan, W. S., Butt, F. K., and Mahmood, A. (2014). Effect of the morphology of CuS upon the photocatalytic degradation of organic dyes. *RSC Advances, 4*(108), 63447-63456.

Tauc, J. (1968). Optical properties and electronic structure of amorphous Ge and Si. *Materials Research Bulletin, 3*(1), 37-46.

Thuy, U. T. D., Liem, N. Q., Parlett, C. M. A., Lalev, G. M., and Wilson, K. (2014). Synthesis of CuS and CuS/ZnS core/shell nanocrystals for photocatalytic degradation of dyes under visible light. *Catalysis Communications, 44*, 62-67.

Tsai, W. T., Hsien, K. J., Chang, Y. M., and Lo, C. C. (2005). Removal of herbicide paraquat from an aqueous solution by adsorption onto spent and treated diatomaceous earth. *Bioresource Technology, 96*(6), 657-663.

Wang, H., Zhang, L., Chen, Z., Hu, J., Li, S., Wang, Z., Liu, J., and Wang, X. (2014a). Semiconductor heterojunction photocatalysts: design, construction, and photocatalytic performances. *Chemical Society Reviews, 43*(15), 5234-5244.

Wang, N., Zheng, T., Zhang, G., and Wang, P. (2016). A review on Fenton-like processes for organic wastewater treatment. *Journal of Environmental Chemical Engineering, 4*(1), 762-787.

Wang, Y., Zhang, L., Jiu, H., Li, N., and Sun, Y. (2014b). Depositing of CuS nanocrystals upon the graphene scaffold and their photocatalytic activities. *Applied Surface Science, 303*, 54-60.

Xu, W., Zhu, S., Liang, Y., Li, Z., Cui, Z., Yang, X., and Inoue, A. (2015). Nanoporous CuS with excellent photocatalytic property. *Scientific Reports, 5*, 18125.

Xu, Y., and Schoonen, M. A. A. (2000). The absolute energy positions of conduction and valence bands of selected semiconducting minerals. *American Mineralogist* (Vol. 85, pp. 543).

Yan, X., Michael, E., Komarneni, S., Brownson, J. R., and Yan, Z.-F. (2013). Microwave- and conventional-hydrothermal synthesis of CuS, SnS and ZnS: Optical properties. *Ceramics International, 39*(5), 4757-4763.

Zhang, J., and Zhang, Z. (2008). Hydrothermal synthesis and optical properties of CuS nanoplates. *Materials Letters, 62*(15), 2279-2281.

Zhang, T., Oyama, T., Aoshima, A., Hidaka, H., Zhao, J., and Serpone, N. (2001). Photooxidative N-demethylation of methylene blue in aqueous TiO2 dispersions under UV irradiation. *Journal of Photochemistry and Photobiology A: Chemistry, 140*(2), 163-172.

Zhuang, T.-T., Fan, F.-J., Gong, M., and Yu, S.-H. (2012). Cu1.94S nanocrystal seed mediated solution-phase growth of unique Cu_2S-PbS heteronanostructures. *Chemical Communications, 48*(78), 9762-9764.